AD-A234 577

(2)

GL-TR-90-0199

NUMERICAL SIMULATION OF QUARRY SOURCE AND REFLECTION/REFRACTION SEISMIC EXPERIMENTS

Gregory L. Wojcik
David K. Vaughan
Harley M. Benz

WEIDLINGER ASSOCIATES
4410 El Camino Real, Suite 110
Los Altos, CA 94022

DTIC
ELECTE
APR 16 1991
C

1 August 1990

Final Report
October 1988 — September 1989

APPROVED FOR PUBLIC RELEASE; DISTRIBUTION UNLIMITED

GEOPHYSICS LABORATORY
AIR FORCE SYSTEMS COMMAND
UNITED STATES AIR FORCE
HANSCOM AIR FORCE BASE, MASSACHUSETTS 01731-5000

DTIC COPY

"This technical report has been reviewed and is approved for publication"

JAMES F. LEWKOWICZ
Contract Manager

JAMES F. LEWKOWICZ
Branch Chief

FOR THE COMMANDER

DONALD H. ECKHARDT
Division Director

This report has been reviewed by the ESD Public Affairs Office (PA) and is releasable to the National Technical Information Service (NTIS).

Qualified requestors may obtain additional copies from the Defense Technical Information Center. All others should apply to the National Technical Information Service.

If your address has changed, or if you wish to be removed from the mailing list, or if the addressee is no longer employed by your organization, please notify GL/IMA, Hanscom AFB, MA 01731. This will assist us in maintaining a current mailing list.

Do not return copies of this report unless contractual obligations or notices on a specific document requires that it be returned.

UNCLASSIFIED

SECURITY CLASSIFICATION OF THIS PAGE

REPORT DOCUMENTATION PAGE

1a REPORT SECURITY CLASSIFICATION Unclassified	1b RESTRICTIVE MARKINGS
2a SECURITY CLASSIFICATION AUTHORITY 2b DECLASSIFICATION/DOWNGRADING SCHEDULE	3 DISTRIBUTION/AVAILABILITY OF REPORT Approved for public release, distribution unlimited
4 PERFORMING ORGANIZATION REPORT NUMBER(S) FR9069	5 MONITORING ORGANIZATION REPORT NUMBER(S) G L TR-90-0199
6a NAME OF PERFORMING ORGANIZATION Weidlinger Associates 6b OFFICE SYMBOL (If applicable)	7a NAME OF MONITORING ORGANIZATION Geophysics Laboratory
6c ADDRESS (City, State, and ZIP Code) 4410 El Camino Real, Suite 110 Los Altos, CA 94022	7b ADDRESS (City, State, and ZIP Code) Hanscom Air Force Base, MA 01731-5000
8a NAME OF FUNDING/SPONSORING ORGANIZATION Geophysics Laboratory 8b OFFICE SYMBOL (If applicable)	9 PROCUREMENT INSTRUMENT IDENTIFICATION NUMBER F19628-88-C-0067
8c ADDRESS (City, State and ZIP Code) Hanscom Air Force Base, MA 01731-5000	10 SOURCE OF FUNDING NUMBERS PROGRAM ELEMENT NO: 62101F PROJECT NO: 7600 TASK NO: 09 WORK UNIT ACCESSION NO: AJ

11 TITLE (Include Security Classification)
Numerical Simulation of Quarry Source and Reflection/Refraction Seismic Experiments

12 PERSONAL AUTHOR(S)
Gregory L. Wojcik, David K. Vaughan, Harley M. Benz

13a TYPE OF REPORT	13b TIME COVERED	14 DATE OF REPORT (Year, Month, Day)	15 PAGE COUNT
Final	FROM 10/88 TO 09/89	1 August 1990	74

16 SUPPLEMENTARY NOTATION

17 COSATI CODES			18 SUBJECT TERMS (Continue on reverse if necessary and identify by block number)
FIELD	GROUP	SUB-GROUP	Seismic modeling, explosion seismology, San Vel Quarry, Ripple-firing, PACE experiment, Crustal structure, PmP, seismic scattering, stochastic modeling, finite element modeling.

19 ABSTRACT (Continue on reverse if necessary and identify by block number)

This final report presents results from numerical simulations of two recent field experiments, the 1987 San Vel Quarry source experiment in Littleton, Massachusetts, and the 1987 PACE reflection/refraction experiment in Arizona. The purpose of this modeling exercise is to explore the use of large-scale simulation as an aid in interpreting such experiments and/or planning similar source and reflection/refraction studies in the future.

The San Vel Quarry simulation is intended to provide insight into conventional quarry blast source effects in terms of shot location and sequencing, as well as local topography and geology. The principal issue addressed is the practicality of using large-scale 3-D finite element analysis as a method for both understanding and generalizing quarry-derived near-field data. Large-scale 3-D simulations were done for a hypothetical single shot in the middle of the borehole array and the actual ripple-fired 72 shot event with deterministic sequencing. Comparisons with recorded accelerograms were made at the ten instrument sites. Quantitative agreement was poor although qualitative effects of topography, shielding, and sequencing were well-modeled. (continued)

20 DISTRIBUTION/AVAILABILITY OF ABSTRACT ☐ UNCLASSIFIED/UNLIMITED ☐ SAME AS RPT ☐ DTIC USERS	21 ABSTRACT SECURITY CLASSIFICATION Unclassified
22a NAME OF RESPONSIBLE INDIVIDUAL James F. Lewkowicz	22b TELEPHONE (Include Area Code) (617) 377-3028 22c. OFFICE SYMBOL GL/LWH

DD FORM 1473, 84 MAR — 83 APR edition may be used until exhausted. All other editions are obsolete.

SECURITY CLASSIFICATION OF THIS PAGE
UNCLASSIFIED

19. ABSTRACT (continued)

The PACE experiment simulation is used to explore the nature of scattering inhomogeneities in the lower crust, in particular, structure responsible for the ubiquitous lower crustal reflections commonly observed in extensional regions like the Basin and Range or the Rhine Graben Modeling reflection/refraction data using numerical scattering simulations offers a practical means to investigate this phenomenon Effects of isotropic and anisotropic scatters in the lower crust were simulated using a time-domain, 2-D, elastic finite element code A series of calculations for different scatterer properties was compared to refraction and coincident wide-angle reflection data for shotpoint 21. Clear effects of random medium type and velocity perturbation were seen and used to place constraints on lower crust composition in the southern Basin and Range

TABLE OF CONTENTS

INTRODUCTION 1

CONCLUSIONS 2

THREE-DIMENSIONAL FINITE ELEMENT SIMULATIONS OF RIPPLE-FIRED QUARRY BLASTS

1. Introduction 3
2. Experiment 4
3. Finite Element Model 7
4. Calculations 8
5. Comparisons 13
6. Conclusions 19

References 20

BASIN AND RANGE CRUSTAL SCATTERING MODELS BASED ON SEISMIC REFLECTION AND REFRACTION DATA

1. Introduction 25
2. Basin and Range Crustal Structure 27
3. Design of the 1987 PACE Seismic Experiment 28
4. Observed Seismic Refraction and Reflection Data 30
5. Finite Element Synthetic Seismograms 34
6. Realization of a Random Velocity Structure 35
7. Finite Element Simulations of the 1987 PACE Seismic Data 37
8. Near-Vertical Reflection Data From SP28 44
9. Discussion and Conclusions 47

Acknowledgements 50

References 51

For
Special
Unannounced
Justification
By
Distribution/
Availability Codes
Avail and/or
Dist Special

INTRODUCTION

This final report presents results from numerical simulations of two recent field experiments, the 1987 San Vel Quarry source experiment in Littleton, Massachusetts, and the 1987 PACE reflection/refraction experiment in Arizona. The purpose of this modeling exercise is to explore the use of large-scale simulation as an aid in interpreting such experiments and/or planning similar source and reflection/refraction studies in the future. The two cases were chosen by virtue of their ongoing interest to Geophysics Laboratory staff and their general relevance to the Test Ban Treaty verification problem.

The San Vel Quarry simulation is intended to provide insight into conventional quarry blast source effects in terms of shot location and sequencing, as well as local topography and geology. Because of overall geometrical and temporal complexity of the physical model, conventional seismic analysis tools are not practical. For example, layered half-space algorithms are inadequate in the near-field due to 3-D source and quarry geometries, while geometrical ray tracing analyses cannot capture the diffracted and surface wave mode converted phases. This leaves discrete numerical simulation as the "best" approach for this study. The principal issue addressed is the practicality of using large-scale 3-D finite element analysis as a method for understanding and generalizing quarry-derived near-field data.

The PACE experiment simulation is used to explore the nature of scattering inhomogeneities in the lower crust. Data from extensive world-wide seismic reflection and refraction profiling efforts have increased our understanding of structure and composition in the crust and upper mantle. However, the structural cause of ubiquitous lower crustal reflections commonly observed in extensional regions, e.g., the Basin and Range or the Rhine Graben, remains unexplained. Modeling reflection/refraction data using numerical scattering simulations offers a practical means to investigate this phenomenon. The 1987 PACE experiment provides an excellent set of refraction and coincident wide-angle reflection data for this purpose. Quantifying the scale-length and magnitude of velocity perturbation in the lower crust is important for establishing petrologic and rheologic constraints, understanding scattering effects on body and surface waves, and separating intrinsic and scattering attenuation.

CONCLUSIONS

Regarding the San Vel Quarry simulations, it is clear that virtually all of the observed phenomenology can be included, at least qualitatively, in the simulation using a large-scale, explicit finite element code without overtly "tuning" the model. Unfortunately, the size and operational complexity of the basic calculation on the Cray-2 makes the requisite suite of simulations prohibitively expensive in terms of cpu time and data post-processing—certainly well beyond the resources available for this project. The multi-borehole source region model contributes much of the simulation's size and complexity, but the necessary transfer of large amounts of synthetic data to a remote site and its processing are the largest drain on resources by a factor of five or more.

The PACE reflection/refraction simulations have clearly demonstrated that elastic waves are sensitive to the type of random media, when viewed over a wide-ranges of incidence angles. The incidence wave and coda behave differently to differences in the random media, e. g., isotropic versus anisotropic small-scale heterogeneities. Further understanding of elastic wave scattering in the crust requires high resolution recordings of seismic data at near-vertical to wide-angles. Coherency analysis of both the direct wave (e.g., the PmP phase) and coda, as a function of offset and frequency, are necessary to constrain possible models of small-scale velocity heterogeneities Furthermore, a comprehensive understand of crustal scale-lengths and attenuation requires a better understanding of the differences observed in both the back-scattered P- and S-wavefields.

THREE-DIMENSIONAL FINITE ELEMENT SIMULATIONS OF RIPPLE-FIRED QUARRY BLASTS

Gregory L. Wojcik and David K. Vaughan
Weidlinger Associates, Los Altos, California

1. Introduction

This paper describes some numerical model simulations of the San Vel Quarry experiment in Littleton, Massachusetts, performed during the summer of 1987 by Stump, et al. (1987) and GL, MIT, and Boston College researchers. These simulations are intended to support continuing field work on the interpretation of quarry explosion source effects as they pertain to Test Ban Treaty verification issues. The work has been performed under an ongoing research program on seismic wave modeling for experiments conducted under the auspices of the Geophysics Laboratory, GL Contract #F19628-88-C-0067.

The ultimate aim of this work is to gain a better understanding of conventional quarry blast source effects in terms of shot distribution and sequencing, as well as local topography and geology. There are a number of approaches available to us for understanding this complex phenomenon including 1) conventional layered half-space interpretation, 2) field data acquisition and interpretation, 3) physical model experiments, and 4) numerical experiments Since the quarry is three-dimensional with a very nonuniform surface, i.e., a big hole in bedrock, conventional half-space methods are inadequate in the near-field, leaving field data and models as the best source of insight.

The principal issue addressed here is the practicality of using large-scale, 3-D finite element model analysis as a method for both understanding and generalizing quarry-derived near-field data. Although high-resolution, large-scale 2-D models are readily analyzed on today's supercomputers, comparable 3-D models typically require at least an order of magnitude greater resources in terms of memory and speed. However, the present quarry problem requires an intermediate model size and level of complexity that should be

practical on a modern machine like the Cray-2. On the other hand, the complexity of the source region, in terms of sequentially detonated multi-boreholes, is an extremely challenging problem.

2. Experiment

The physical experiment measured ground acceleration and/or velocity at ranges of hundreds of meters to tens of kilometers from a series of quarry blasts at the San Vel Quarry in Littleton, Massachusetts. The blasts were conventional quarrying explosions intended to fracture and rubbleize rock off one of the quarry pit's faces. The pit itself was approximately 400x800x60 feet at the time of the experiments. The typical blast configuration consisted of three staggered rows of explosive-filled bore holes (48-72 total), each approximately 58-60 feet deep, along a portion of the pit's edge. The holes were detonated in succession along the edge, so-called ripple firing, with the detonation sequence (delay time) chosen empirically to maximize rock fracturing while minimizing ground motions felt by nearby homes and businesses. Although seismic data were collected at various ranges, the set of principal interest here are accelerograms from instruments scattered around the pit within a circle approximately 1600 feet in diameter. Locations are shown in Fig. 1 and an example of the shot array geometry and ideal firing sequence is given in Fig. 2. The three-component acceleration records at the sites are given in Stump, et al. (1987). Three blasts, each on a different section of the pit perimeter, were recorded at these instrument sites.

One purpose of the experiment was to examine effects of ripple firing on ground motion spectra. This type of detonation produces spectral scalloping that may be useful in discriminating small nuclear explosions from quarry blasts. It was noted, in both these as well as other experiments, that the actual delay times deviated significantly from those planned—apparently caused by repeatability problems with commercial blasting caps. The question is what effect do these random delay time errors and local site effects have on ground motion, and spectral scalloping in particular? Since this is difficult to answer in the field, our research approaches the problem by means of numerical modeling. The objective is to numerically simulate the detonation sequence in a discrete model of the quarry, generate a set of synthetic seismograms at the

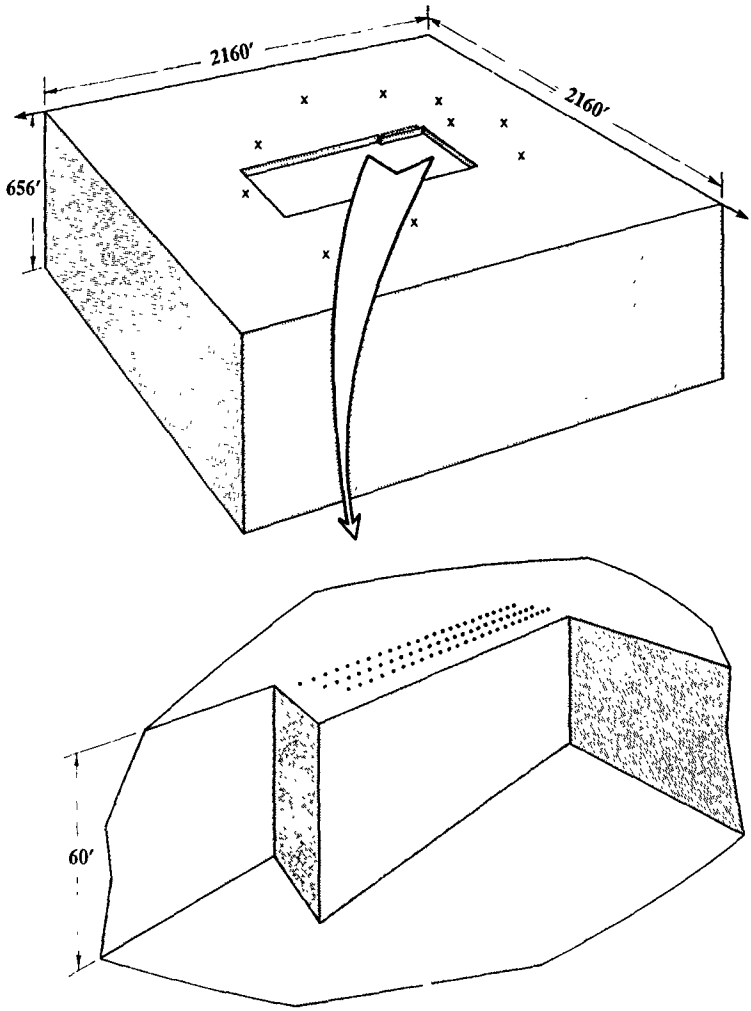

Figure 1. An illustration of the three-dimensional quarry model showing dimensions, instrument locations and a detail of the explosive borehole array.

SHOT 3

SAN VEL QUARRY

7 / 29 / 87

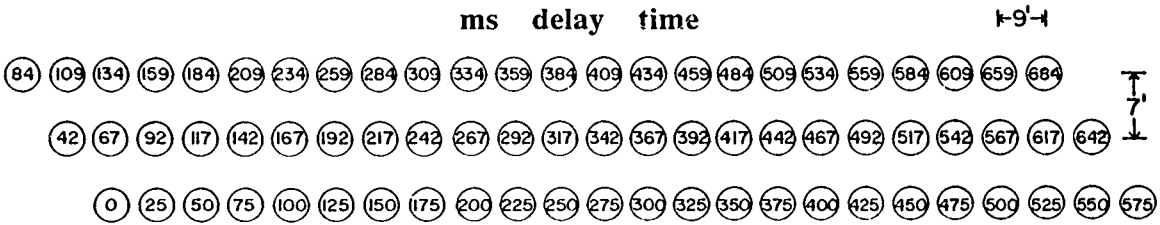

Total Lbs: 24350
Max Holes/Delay: 2
Max Lbs/Delay: 696
Hole Depth: 58' - 60'
Stemming: 4' - 8.5'

Quarry Face

Figure 2. The borehole array geometry and exact firing sequence for Shot 3.

scaled instrument locations, and compare synthetic and measured seismograms. The calculations are expected to yield insight into effects of shot timing errors and local topography and geology on observed ground motions.

3. Finite Element Model

To perform the simulations, a three-dimensional, explicit finite element model of the quarry was built and executed on a Cray-2 supercomputer at the Air Force Weapons Laboratory. The 240 x 240 x 74 element model (= 4.6 million elements including source region refinement) represented the quarry pit and surrounding area (2160 x 2160 x 656 feet) including all accelerometer sites. It was gridded to propagate 100 Hz shear (S-)waves without significant dispersion, since this was the upper bound on instrument frequency response.

The model required significant new code development in order to accommodate the large number of small-diameter, explosive filled bore holes. Since the typical hole was much smaller than a free-field element, a subgridding capability was developed to grade the grid size down from the free-field dimension, through an intermediate zone, to approximately twice the hole diameter.

Because the quarry blast is highly nonlinear near the explosive array—due to high pressure, fracturing, and the resulting large strains and displacements—conventional linear source modeling techniques could not be used. Instead an "energy pill" source was implemented, where the explosive cylinder and its immediate neighborhood was replaced after detonation by a pressurized, outwardly moving region with one percent of the total energy (1/2 kinetic plus 1/2 potential) as the explosive products and included rock. Nonlinear rock fracturing was mimicked by tension cutoff in the element's material model. A nonlinear cap model of the inelastic constitutive behavior of rock was considered initially but never implemented due to the dominance of fracturing, rather than cyclic nonlinear processes. Although the detailed fracture phenomenology is not simulated by this model, it was deemed adequate for calculating the seismic pulses radiated by the explosion, including shielding by fractured rock around neighboring boreholes. A two-

dimensional example of the model soon after detonation of three sheets (i.e., two-dimensional boreholes) of explosive is shown in Fig. 3. This and other 2-D models were used extensively for development of the source and subgrid coding implemented finally in 3-D.

The principal difficulty encountered with the model is late time numerical noise contamination. This is due to the calculation's relatively long duration , about one second of simulated time, and the high frequency nature of the borehole detonations and rock fracturing. Waves reverberate within the model many times over this period, and since the radiation boundary condition (absorbing boundary) on the outer sides of the model is not perfect, trapped energy eventually grows to a significant level. This problem was reduced to the point that reasonable results could be obtained by moving the bottom boundary deeper and introducing a small amount of viscous damping. The damping does not affect the seismic signals significantly, but it does reduce the ringing substantially. Note that the damping introduced is much less than a realistic Q would imply and is only introduced for numerical purposes. This experience clearly indicates the need for better time-domain radiation boundary conditions.

4. Calculations

Two calculations were done on the full 3-D model. The first was hypothetical and assumed a single borehole explosion in the center of the Shot 3 array. The second was a full simulation of the Shot 3 configuration with 72 borehole explosions detonated according to the original delay time specifications. The latter simulation used about 33 hours of CPU time to simulate one second of model response, and required 90 million words of memory. Synthetic vertical velocity seismograms on a circle surrounding the Shot 3 array and on lines through the array, perpendicular and parallel to the quarry face are shown in Figures 4-9.

Figures 4-6 show the single shot synthetic seismograms. Figure 4 illustrates the influence of quarry topography on the azimuthal distribution of ground motion. Arrival times at 180° to 360° indicate a prominent P-wave arrival followed by S-waves and the dominant Rayleigh wave. The P-wave at

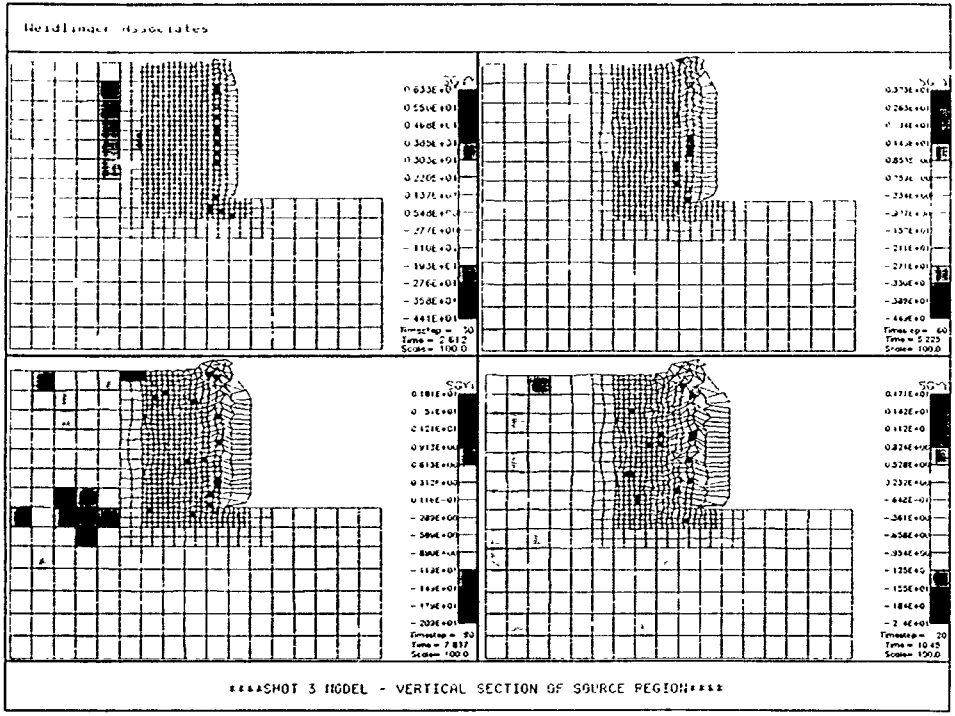

Figure 3. A two-dimensional example of the source region finite element model with grid refinement, showing a sequence of snapshots after detonation of three borehole lines (sheets).

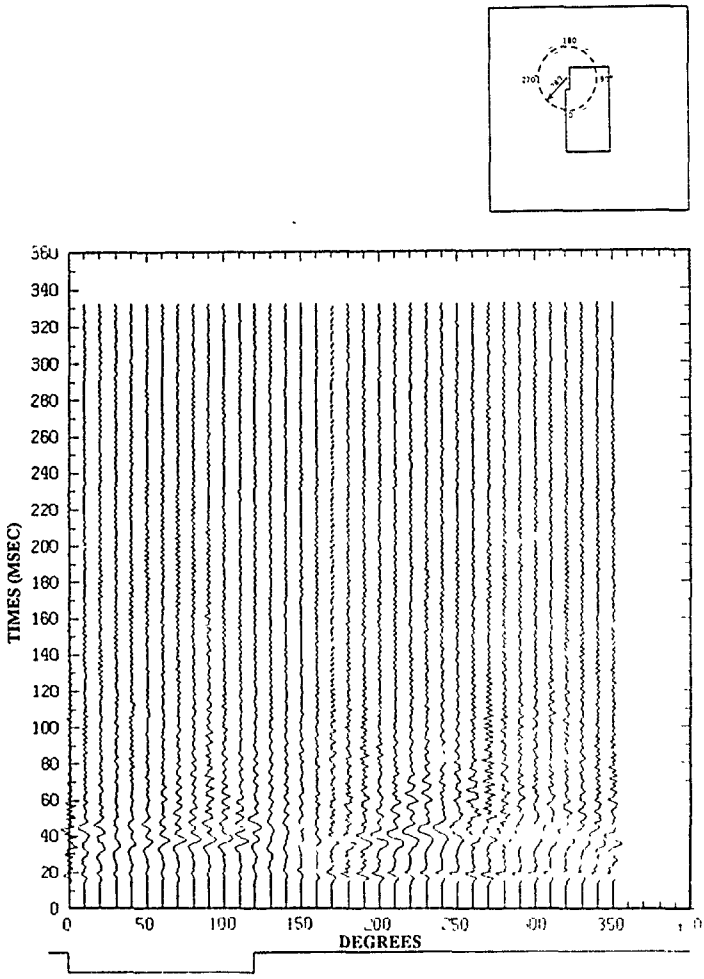

Figure 4. Calculated vertical velocity seismograms at a radius of 280 feet, for a single shot at the center of the Shot 3 borehole array.

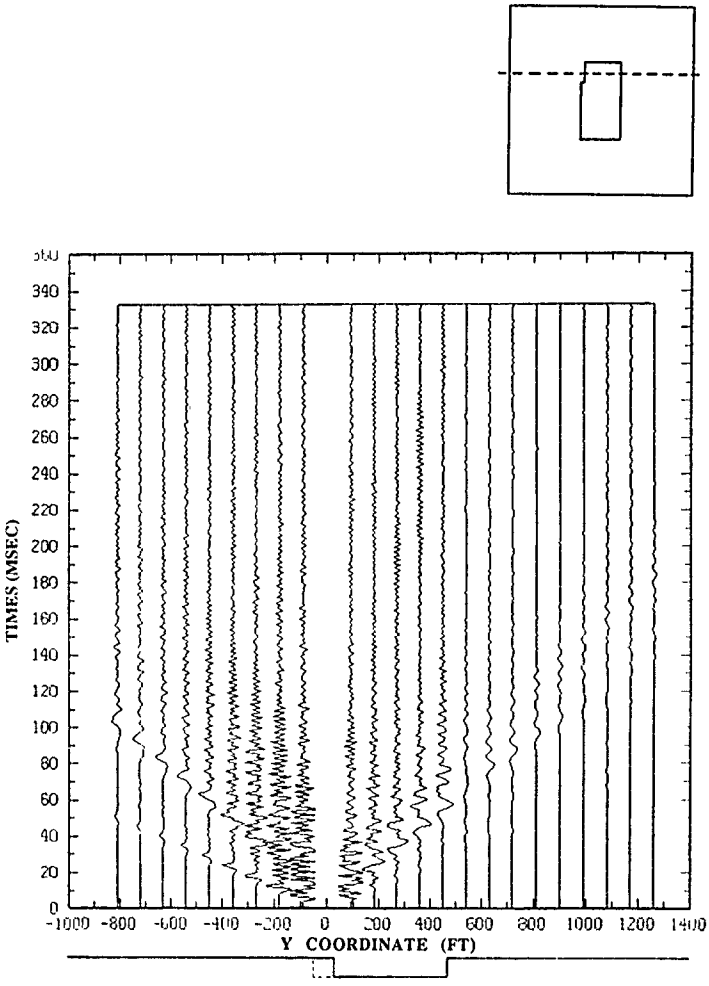

Figure 5. Calculated vertical velocity seismograms on a line perpendicular to the Shot 3 quarry face for a single shot.

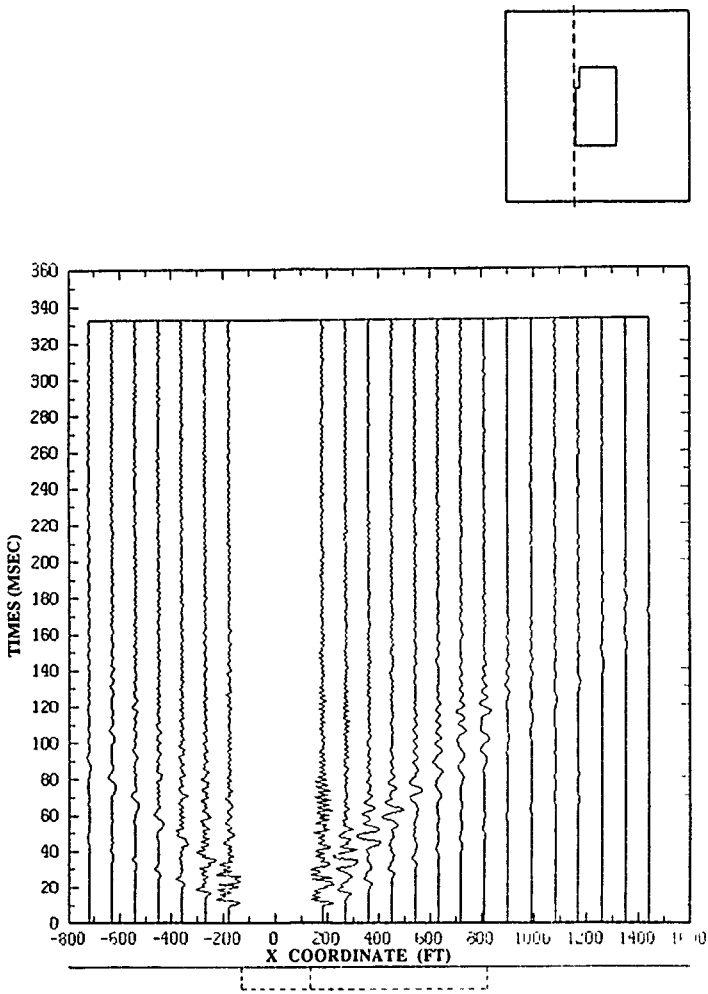

Figure 6. Calculated vertical velocity seismograms on a line parallel to the Shot 3 quarry face for a single shot.

0° to 150° is a much weaker arrival due to shielding by the quarry faces. Apparently, the S- and Rayleigh waves are not shielded except along azimuths from 130° to 160°, corresponding to the corner of the quarry. Figures 5 and 6 illustrate the decay of arrivals with distance from the shot. Figure 5 in particular shows shielding of the P-wave by the quarry faces and a relative time delay for the Rayleigh wave on the left side of the quarry. It also indicates significantly stronger motion on the quarry floor than outside on the natural ground level, probably due to shielding by the right quarry face.

Figures 7-9 show corresponding synthetic seismograms for the 72 ripple-fired shots. The duration necessary to capture the complete sequence (≈0.8 s) appears to be given by the single shot duration (≈0.14 s) plus the sequence time (≈0.7 s). Complexity of these seismograms is clearly much greater than for the single shot, with motion dominated by Rayleigh waves from the long sequence of explosions. Note that in Fig. 7, the azimuthal distribution of amplitudes is similar to that in Fig. 4, corresponding to the shielding noted above. However, the timing of highest ground motion at any azimuth is directly related to proximity and timing of the shot sequence, e.g., the strong arrivals from 170° to 200° at 0.4 s to 0.6 s correspond to the later shots located closest to these output points, e.g., see Fig. 2. Similar conclusions follow from Figures 8 and 9. There does not appear to be any directivity effect due to shot interference, particularly since the sequencing would be designed to prevent constructive interference.

5. Comparisons

Locations of the ten accelerometer locations around the quarry are shown in Fig. 10. Comparisons of measured and synthetic seismograms at these stations are made in Figures 11-15. Figure 11 compares arrival times, durations, and vertical accelerations at two instrument locations on the left and right sides of the quarry. Note that synthetic acceleration was obtained by differentiating velocity. Significant errors in both timing, duration, and amplitudes are seen. However, the arrival time comparison is invalid because the measured times are inconsistent with the instrument distances from the shot array. The amplitudes are in reasonable agreement at Gauge 3 but the calculations overpredict acceleration at Gauge 7. Although truncated by the

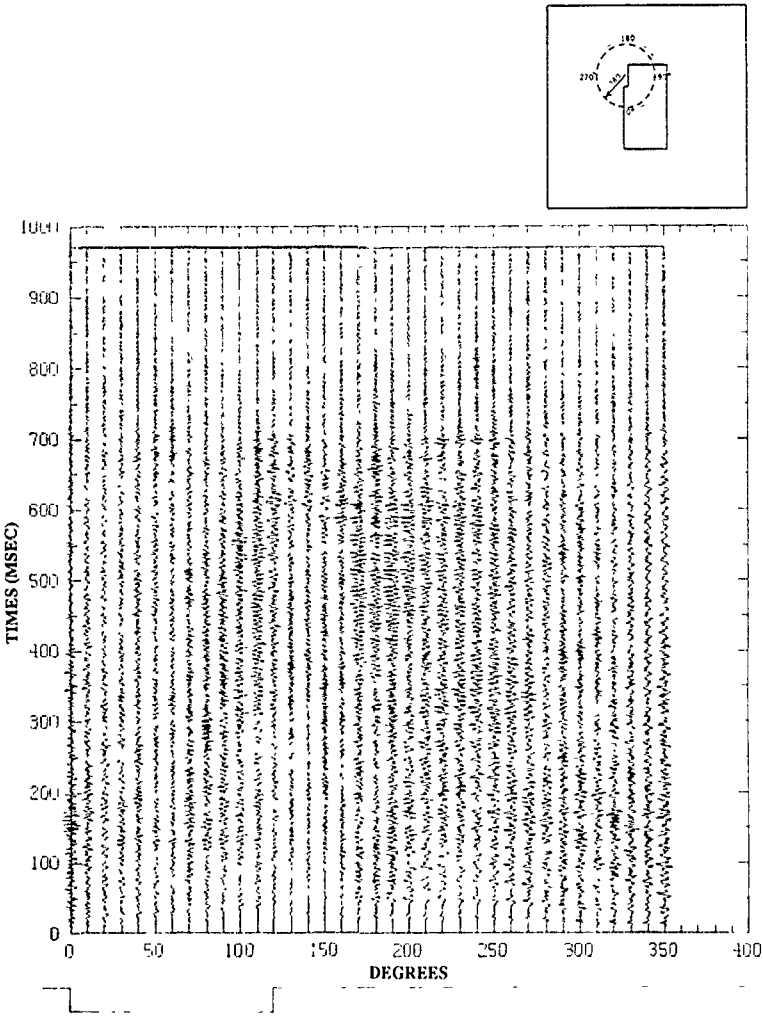

Figure 7. Calculated vertical velocity seismograms at a radius of 280 feet from the center of the Shot 3 borehole array for the 72 ripple-fired shots.

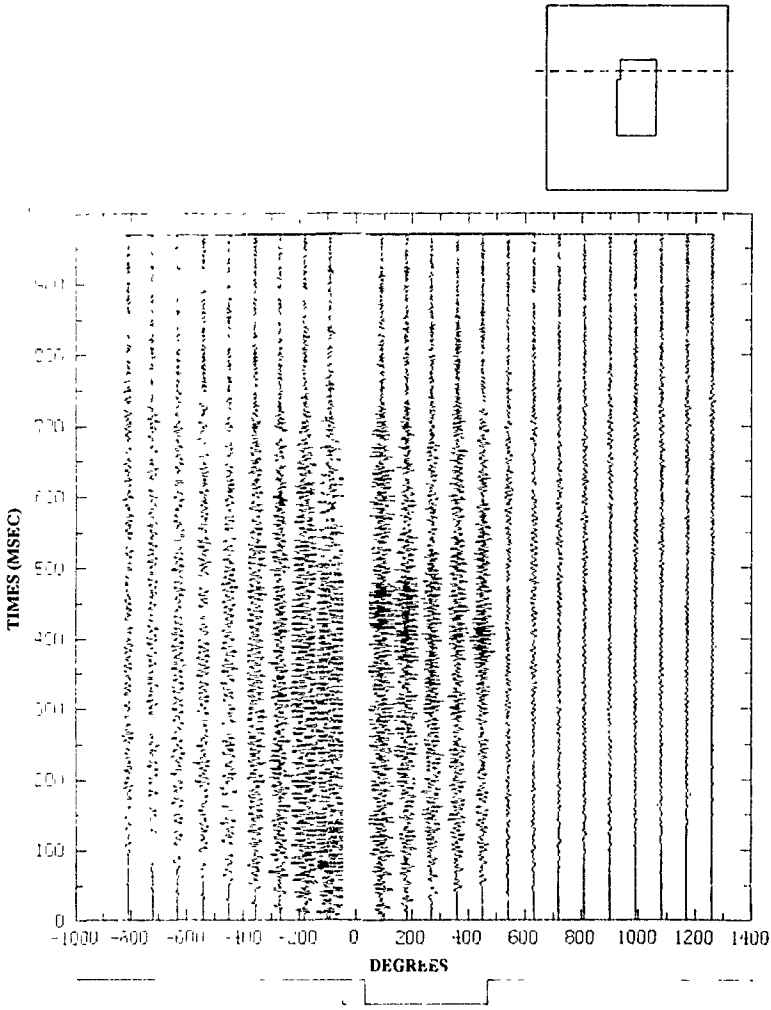

Figure 8. Calculated vertical velocity seismograms on a line perpendicular to the Shot 3 quarry face for the 72 ripple-fired shots.

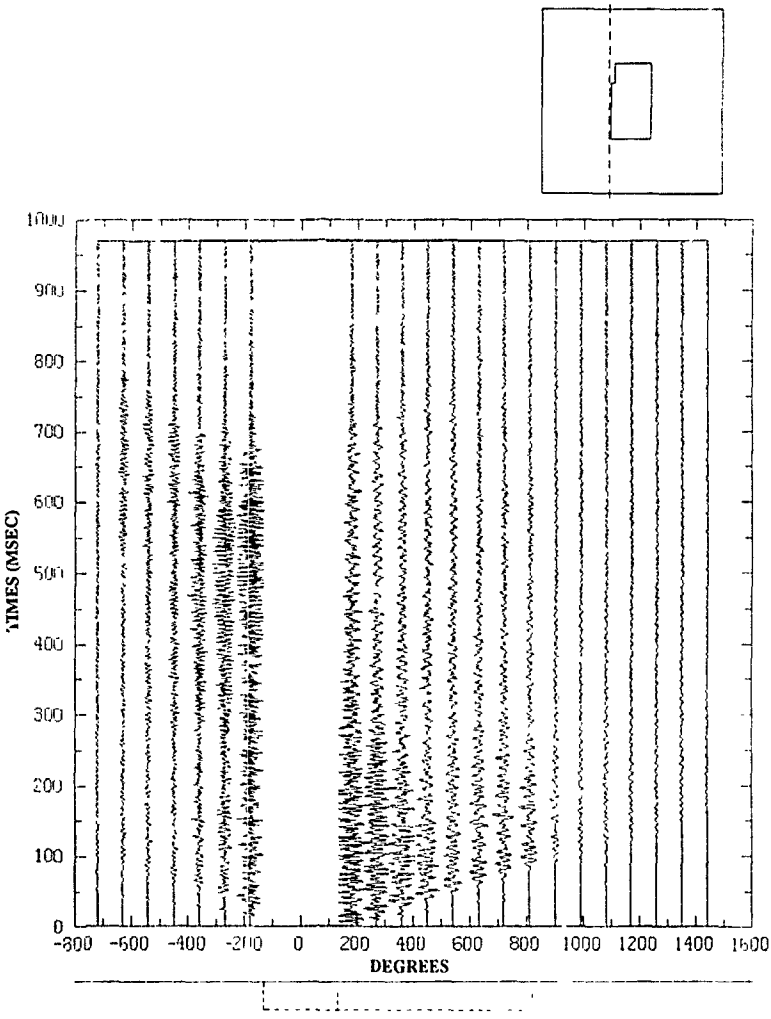

Figure 9. Calculated vertical velocity seismograms on a line parallel to the Shot 3 quarry face for the 72 ripple-fired shots.

SAN VEL QUARRY ACCELEROMETERS

LITTLETON, MA 1987

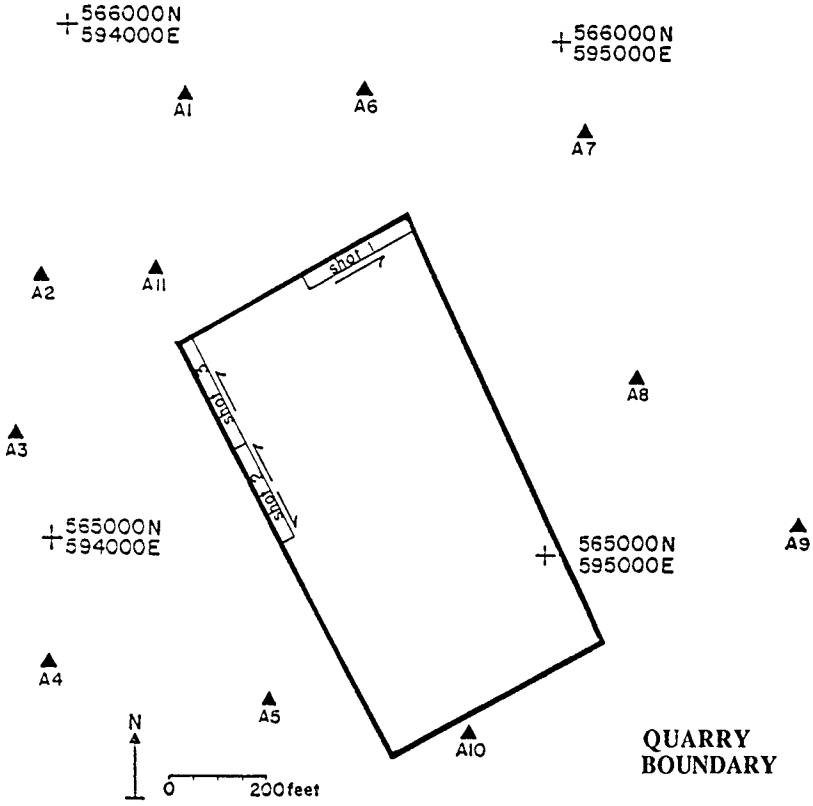

Figure 10. Locations of accelerometers around the quarry.

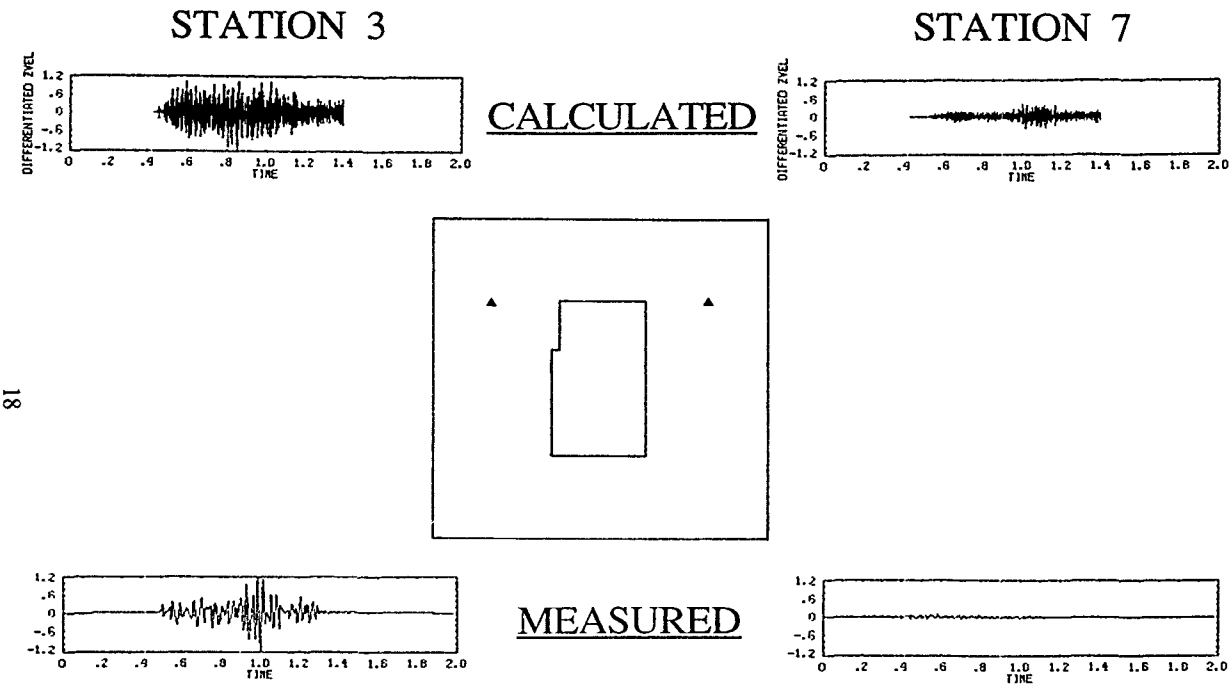

Figure 11. Examples of calculated and measured acceleration histories for Shot 3.

need to terminate the calculation, the durations are too long in the calculation, probably due to the lack of a realistic amount of material damping.

Figures 12-14 compare synthetic velocity seismograms—vertical, north, and east respectively—with recorded velocities (integrated accelerations) at the instrument sites. The amplitude ration is indicate between the two sets of time histories. In all cases, the calculated velocities are too low. This is not surprizing considering that the energy coupling coefficient was arbitrarily taken as 0.01 and could be significantly higher. Increasing this coefficient would not increase all of the output stations uniformly due to the nonlinear tension cutoff process in the source region. The monochromatic appearance of the calculation is due to the assumption of uniform shot sequencing. A more realistic random pattern would introduce significant interference between the arrivals.

Figure 15 compares synthetic and measured spectra at the two sites on either side of the quarry shown in Fig. 10. It is clear that there is relatively more high frequency motion in the synthetics than in the data. This is an artifact of the calculation's very severe, high frequency source environment, and inadequate damping—both intrinsic and scattering-induced—in the source region and on the travel path.

6. Conclusions

Our conclusion from this comparison is that over-all similarities between calculation and experiment may exist for azimuthal or distance variations due to gross shielding, but quantitative comparison is poor in general. Better phenomenological modeling is clearly needed in the source region, including a better estimate of the source coupling coefficient. This refined source model may require a subgrid with a few million elements alone. In addition, intrinsic damping should be included along with a weathered layer, i.e., a high near-surface velocity gradient. At the least, a suite of elastic calculations should have preceded those presented here in order to obtain better insight into shot sequencing and topographic effects.

These results indicate to us the practicality, albeit limited, of 3-D numerical simulations in local geology and topography as an aid in interpreting and perhaps generalizing field data. However, it is clear that only gross behavior can be deduced from calculations, i.e., one-to-one comparisons with field measurements are virtually impossible. Furthermore, the full suite of calculations that would be required for an investigation of shot timing errors on spectra and signal interference are prohibited by the limited run time available on the Cray-2 used for this study. Hundreds of hours would be necessary for a more complete study.

In addition to studies of seismic arrivals on the surface, it would be of interest to examine the distribution of downgoing energy as a means to predict the far-field radiation pattern. This can certainly be done, even with the vertically truncated model used in this study. The difficulty is the limited capability for transferring large amounts of data from a remote Cray-2 facility to the analyst's office. Although possible, in practice, limited postprocessing budgets currently limit such studies to onsite researchers who have direct access to a large data space.

References

Stump, B.W., S.K. Reamer, R.E. Reinke, and J.A. Leverette, and R. Goerke (1987). SAN VEL QUARRY EXPERIMENT: Near-Source Data, Dept. of Geological Sciences, Southern Methodist University, Dallas, TX 75275.

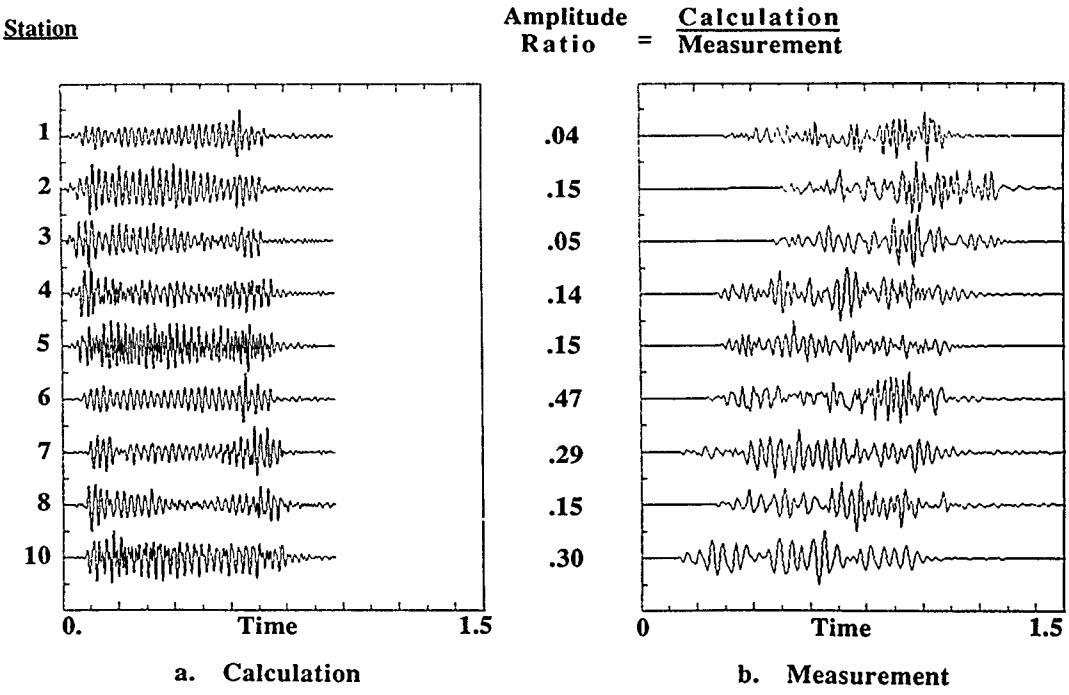

Figure 12. Comparison of calculated and measured vertical seismograms in and around the quarry for Shot 3.

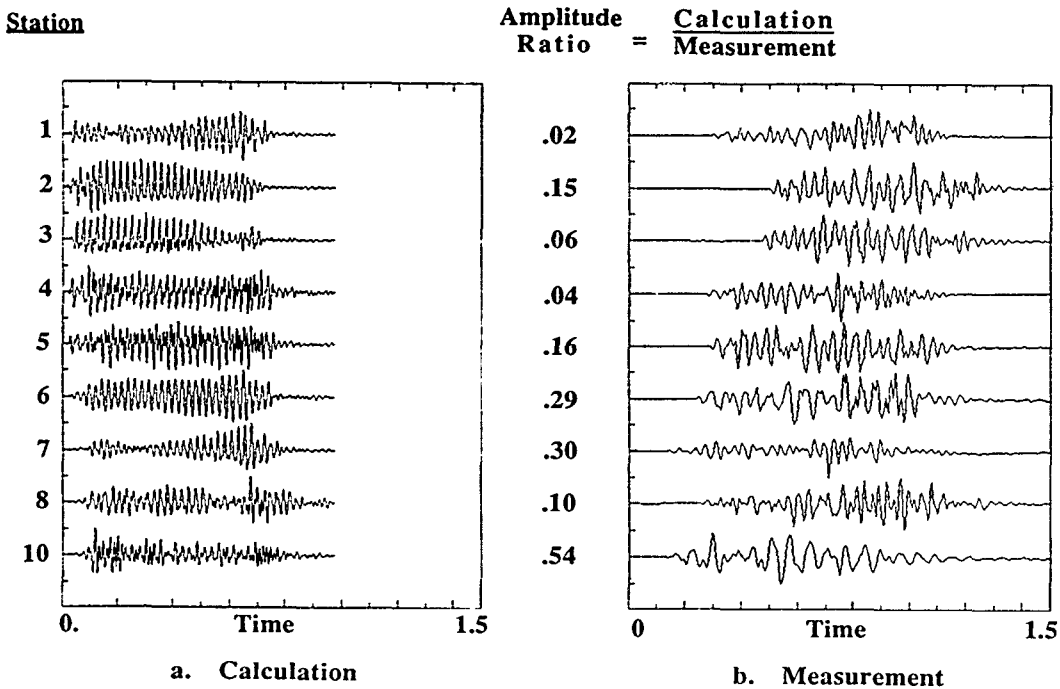

Figure 13. Comparison of calculated and measured north-south seismograms in and around the quarry for Shot 3.

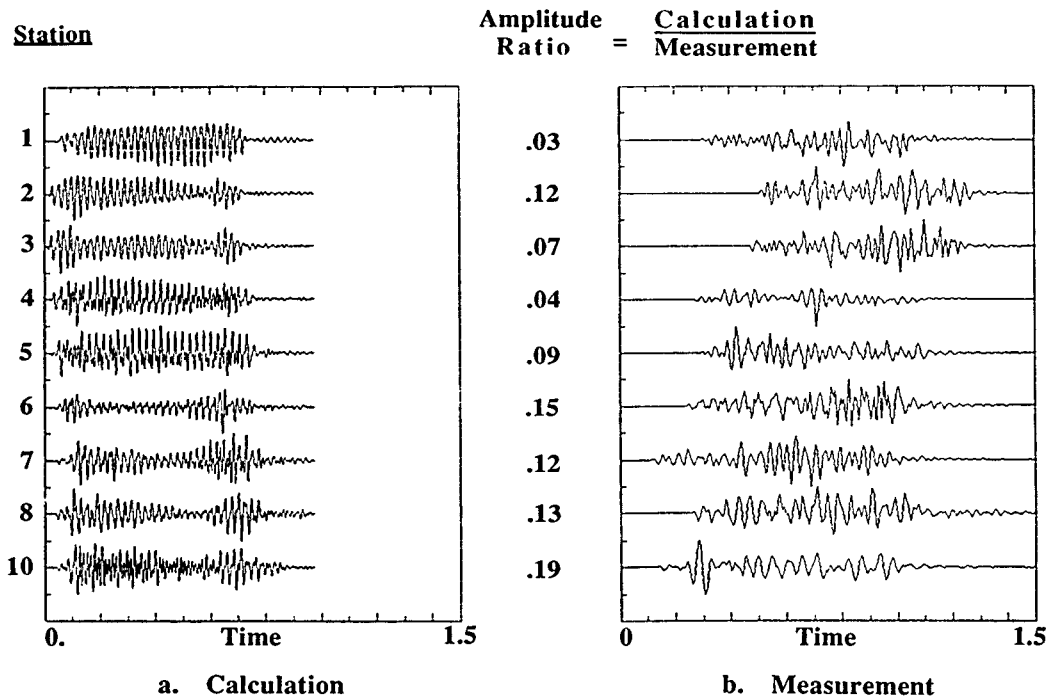

Figure 14. Comparison of calculated and measured east-west seismograms in and around the quarry for Shot 3.

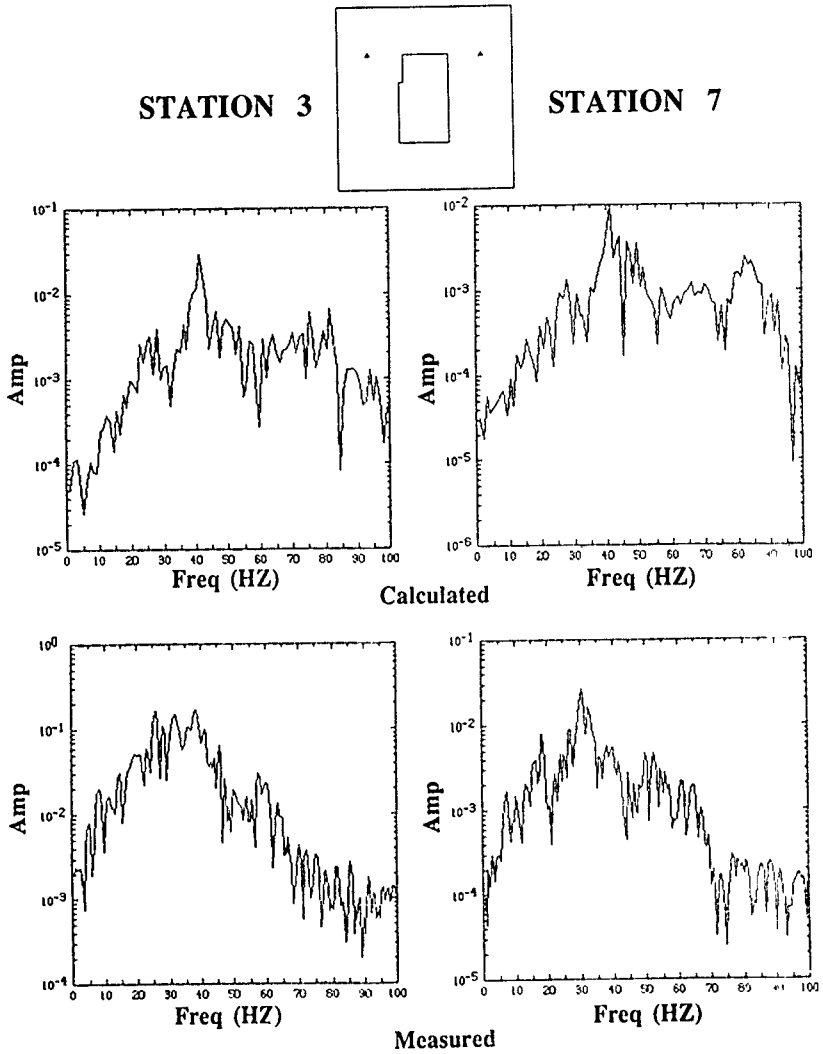

Figure 15. Comparison of calculated and measured frequency spectra for Stations 3 and 7.

BASIN AND RANGE CRUSTAL SCATTERING MODELS BASED ON SEISMIC REFLECTION AND REFRACTION DATA

Harley M. Benz
U. S. Geological Survey, Menlo Park, California

David K. Vaughan
Weidlinger Associates, Los Altos, California

Gregory L. Wojcik
Weidlinger Associates, Los Altos, California

1. Introduction

Over the past decade, extensive world-wide seismic reflection and refraction profiling efforts have added considerably to our understanding of structure and composition in the crust and upper mantle. In certain regions this work has increased resolution of deeper crustal structure to features on the order of a few wavelengths, although many questions remain unanswered concerning the physical nature of these structures.

Of particular interest is the structural source of ubiquitous lower crustal reflections commonly observed in extensional regions, e.g. the Basin and Range and Rhine Graben. Modeling reflection/refraction data using numerical scattering simulations offers a practical means to investigate this phenomenon. However, the likelihood of both lateral and vertical crustal inhomogeneity in a realistic model makes such simulation difficult, if not impossible, using traditional approaches. This paper investigates the problem using stochastic finite element models of the crust and upper mantle.

To address the effects of crustal scattering on refraction/wide-angle reflection data, we model selected refraction data [*McCarthy et al.*, 1990] and coincident reflection data [*Goodwin and McCarthy*, 1990] recorded across the Buckskin-Rawhide Mountains metamorphic core complex in the southern Basin and Range. Stochastic models of lower crustal velocity structure are used to simulate high frequency (> 5 Hz) elastic wave propagation in order to

determine how prominent crustal P-wave phases are affected by small scale crustal heterogeneities. Quantifying the scale-length and magnitude of velocity fluctuation in the lower crust is important for: 1) establishing petrologic and rheologic constraints based on models of admissible velocity variations; 2) understanding the role of crustal heterogeneities on body and surface wave transmission; and 3) determining differences between intrinsic and scattering attenuation. The first two objectives are accomplished here by deterministic and stochastic finite element synthetic seismogram modeling of the coincident near-vertical reflection data and the wide-angle refraction data. The deterministic two-dimensional velocity models used in the finite element simulations was derived from detailed travel time and amplitude analysis of the 1987 refraction data [*McCarthy et al.*, 1990].

By way of background, reflectivity and finite difference synthetic seismogram techniques have recently used novel approaches to simulate lower crustal reflectivity [*Sandmeier et al.*, 1987; *Gibson and Levander*, 1988]. Modeling refraction data from the Rhine Graben, *Sandmeier and Wenzel* [1987] simulated lower crustal reflectivity using a velocity model consisting of a series of random plane layer thicknesses that alternated between high and low velocities. Multiple reverberations within the finely layered lower crust produces the complex coda seen in wide-angle refraction data.

Gibson and Levander [1988] explained the same features by using a quite different velocity model that contained random isotropic velocity variations in the lower crust. These two models represent what can be considered "end-member" velocity structures that may explain the origins of lower crustal reflectivity. Importantly, each model, based on the dimensions of the crustal scatterers and range of velocity fluctuations, has differing implications about the present state of the lower crust and the processes that form the crust, such as the migration of crustal magma, emplacement of mantle derived melts, and lower crustal ductility.

The origins of body wave coda observed in local earthquake recordings [*Frankel and Clayton*, 1987] and seismic refraction and reflection profiles [*Sandmeier et al.*, 1987; *Gibson and Levander*, 1987] have proven difficult to explain using conventional synthetic modeling techniques. Crust and upper-

mantle structure is quite complex, containing a large range of scale lengths and velocity fluctuations [*Wu and Aki*, 1989] that are difficult to accurately approximate. A variety of synthetic seismogram techniques have been used to model body wave coda. Ray theoretical methods [*Cerveny et al.*, 1982] have been particularly useful for modeling small-angle scattering in two- and three-dimensional structures, where it is assumed that the incident wavelength is much larger than the characteristic length of the structure. Reflectivity synthetic seismograms, limited to depth-dependent variations in velocity, have successfully modeled high-frequency (>20 Hz) elastic wave coda produced by a finely laminated lower crust [*Sandmeier et al.*, 1987]. More general finite-difference simulations of seismic wave propagation in two-dimensional random velocity media [*Frankel and Clayton*, 1984] have been used to constrain the average scattering properties of the crust. Finite difference and finite element methods, are being used more often in coda studies because of their ability to model small-scale heterogeneities and wide-angle scattering. In addition, these techniques are not restricted to body wave propagation but can also accurately simulate surface waves in random media [*Hill and Levander*, 1984].

2. Basin and Range Crustal Structure

Geophysical surveys and geologic interpretations of Basin and Range structure and tectonics constitute a large body of literature. Reviews of the regional geology and geophysics of the Basin and Range include those of *Thompson and Burke* [1974], *Smith* [1978], *Eaton* [1979], *Speed* [1982], *Allmendinger et al.* [1987], *Pakiser* [1989], *Smith et al.* [1989], and *Thompson et al* [1989]. The reader is referred to *McCarthy et al.* [1990] for a description of the regional geology and tectonics in the vicinity of the 1987 PACE experiment.

Since the mid 1960's, extensive refraction profiling of the Basin and Range Province has established that the crust is thin (< 32 km thick) with upper mantle P-wave velocities between 7.8 and 8.1 km s^{-1}. Reinterpretation and summary of USGS seismic refraction data [Prodehl, 1979] suggests a 29 to 35 km crust with a 7.9 km s^{-1} upper mantle velocity. Using Nevada Test Site (NTS) explosions and quarry blasts, *Stauber and Boore* [1978] found evidence

for an anomalously thin crust and low upper-mantle velocity of 7.8 km s^{-1}. Recording independent refraction data, using NTS explosions and quarry blasts, *Priestley et al.* [1982] concluded that the crust in northwestern Nevada is as thin as 20 km. Both *Stauber and Boore* [1978] and *Priestley et al.* [1982] recorded unreversed profiles, hence, their crustal thicknesses and Pn velocities must be considered poorly constrained. Refraction results for northern Nevada [*Benz et al.*, 1990] indicates a crustal thickness of ≈30 km and upper mantle velocities of 7.9-8.0 km s^{-1}, which argues against an anomalous crust in northern Nevada when viewed on a Basin wide average. While details may differ, the southern Basin and Range velocity structure [*McCarthy et al.*, 1990] is similar to that found in Nevada [*Benz et al.*, 1990]. Crustal thickness is ≈30 km and upper-mantle velocities range from 7.9 to 8.0 km s^{-1}. COCORP reflection profiling throughout the Basin and Range [*Allmendinger et al.*, 1987; *Hague et al.*, 1987; *Hague et al.*, 1986] has also revealed: 1) a moderately reflective upper crust with evidence of planar to listric normal faults and asymmetric basins; 2) a highly reflective lower crust marked by sub-horizontal, discontinuous reflections; and 3) a laterally discontinuous, but moderately reflective Moho [*Klemperer et al.*, 1986].

3. Design of the 1987 PACE Seismic Experiment

The 1987 PACE seismic experiment was designed to: 1) image the crustal structure of the Buckskin-Rawhide Mountain metamorphic core complex; 2) determine the crust and upper mantle structure across the Colorado Plateau/Basin and Range transition; and 3) record wide-angle refraction and coincident reflection data with the intent of using the inherent strengths of each technique to improve the resolution of lower crustal structure. Achieving these objectives required deploying a 180 km NE-SW trending refraction profile (Fig. 1) crossing the Buckskin-Rawhide Mountain metamorphic core complex and roughly perpendicular to the regional direction of extension [*Eddington et al.*, 1986]. The profile consists of two 140-km-long deployments laid end-to-end, each including 120 cassette recorders spaced ~750 m apart [*Healy et al*, 1982]. An in-line 400-channel, industry standard reflection array with a station spacing of ~40 m was located between shotpoints 28 and 29 in the transition zone (Fig. 1). Both the refraction and reflection arrays recorded 27 shots from 19 shotpoints.

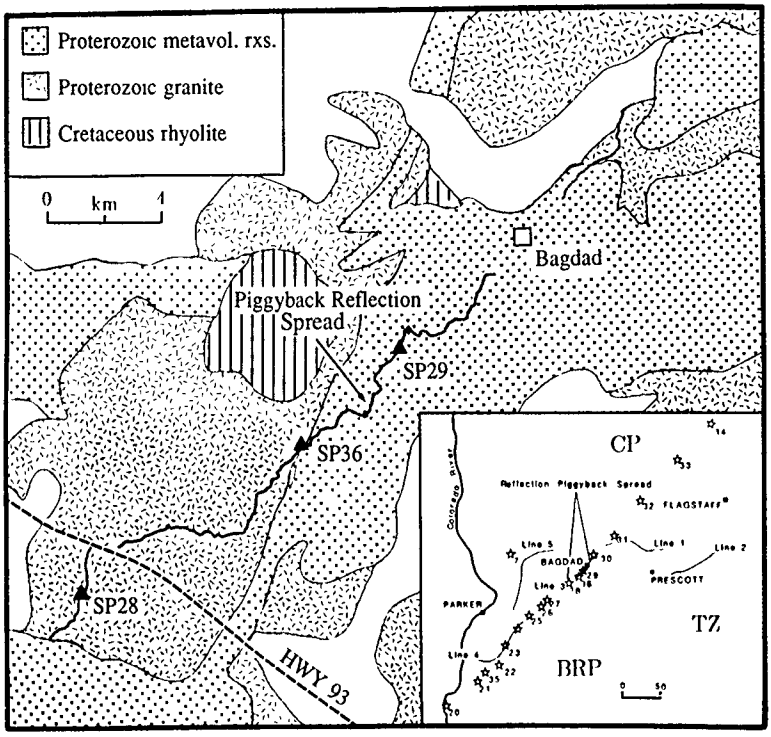

Figure 1. Location map of the 1987 PACE seismic transect. Triangles and stars (inset) are the principal shotpoints (SP) referred to in the discussion. The heavy lines are the location of the coincident reflection arrays. Arizona COCORP profile is shown as solid lines in inset.

Several shotpoints were shot during both deployments in order to increase the maximum recorded offset for the profile. Shots were spaced ~25 km apart and charge sizes ranged from 400 to 2700 kg. Details on the station locations, shot size, and instrumentation used in the refraction recording are given in *Larkin et al.* [1989]. In the remainder of this paper, individual record sections will be denoted by their shotpoint number, e.g., shotpoint 21 will be referred to as SP21.

Our interpretation of the 1987 PACE seismic data focuses on developing a model of crust and upper-mantle structure based on finite element simulation of selected seismic refraction/wide-angle reflection data that we feel characterize the deep crustal structure of the southern Basin and Range. Our discussion complements other studies of the 1987 PACE seismic data including the two-dimensional travel-time and ray-theoretical synthetic-seismogram modeling of *McCarthy et al.* [1990] and the three-component seismic modeling of *Goodwin and McCarthy* [1990].

4. Observed Seismic Refraction and Reflection Data

This paper utilizes amplitude and travel time variations observed in the refraction and coincident reflection arrays to infer detailed characteristics of lower crustal velocity structure. This study focuses exclusively on modeling crustal P-waves, and will primarily address variations in PmP travel time and amplitude in terms of lower crustal structure and scattering. Accurately modeling PmP is particularly important considering it is the most prominent wide-angle phase that propagates through the lower crust, and will be the crustal body-wave phase most sensitive to small-scale velocity heterogeneities. Figure 2 shows the refraction record section (SP21) that will be modeled in this study. Each trace is low-pass filtered to 12 Hz and plotted trace normalized with a reducing velocity of 6.0 km s^{-1}. Time-term corrections were applied to correct for systematic travel-time variations due to velocity changes near the recorder [*Kohler*, 1988]. The time-term correction reduces the data to a datum coincident with the elevation of the source by applying a static travel time shifts to each seismic trace. For the entire profile, time-term corrections averaged -0.08 s and ranged from -0.46 s to +0.25 s.

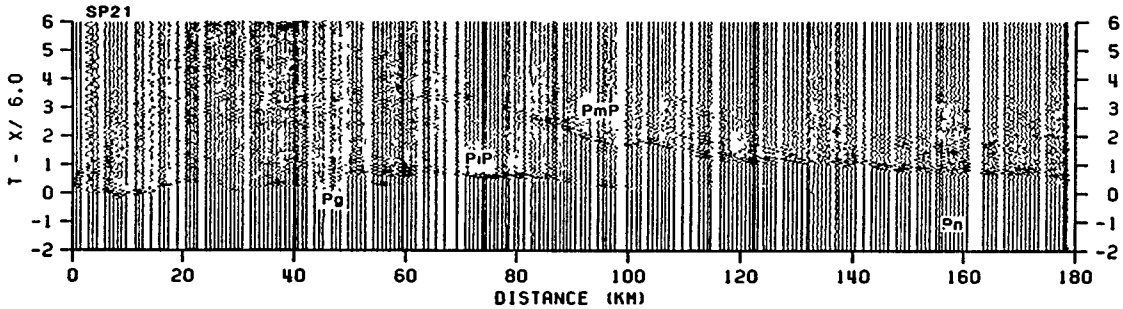

Figure 2. SP21 trace normalized record section. Each trace has been bandpass filtered between 0.1 and 12.0 Hz, time-term corrected to the elevation of the corresponding shotpoint, and plotted using a reducing velocity of 6.0 km s^{-1}. Stations north of the shotpoint are represented by positive distances. Key to phase identifications (used here and in the following figures): Pg, the diving or continuously refracted P wave in the crystalline upper crust; PiP, the wide-angle reflection from the mid-crustal discontinuity; PmP, the wide-angle reflection off the crust-mantle boundary (Moho); and Pn, the upper-mantle head wave.

The prominent crustal P-wave phases easily recognizable on the record section are the upper crustal headwave (Pg), the mid-crustal reflection (PiP), the Moho reflection (PmP), and upper mantle headwave (Pn). The Pg phase is observed and correlatable as a first arrivals to distances greater than 90 km. Large travel time variations of the Pg phase indicate large differences in near-surface velocity structure along the profile. On average, the apparent velocity of the Pg phase is 6.0 km s^{-1}. The mid-crustal reflection (PiP) is observed as a secondary arrival from ≈30 (1.0 s reduced time) to ≈120 km (0.5 s reduced time). The PiP closely following in travel time the Pg phase suggests that the mid-crustal boundary is relatively shallow (<15-18 km), given that the upper crustal basement has a velocity of 6.0 km s^{-1}. This observation is supported by the modeling results of *McCarthy et al.* [1990] that place the mid-crustal boundary at 12 km beneath the center of the profile. Following the mid-crustal reflection, the PmP phase is the most prominent secondary arrival and is observed from ≈70 (≈3.5 s reduced time) to 180 km (0.5 s reduced time). The lack of pre-critical energy (<80 km) may indicate a transitional crust-mantle boundary [*Braile and Smith*, 1977]. The upper-mantle headwave (Pn) is observed as a first arrival starting at ≈140 km (0.0 s reduced time) and is observed to a distance of 170 km (-1.0 s reduced time).

High-quality, single-fold reflection data recorded by the coincident reflection array are shown in Figure 3. The record section is a composite made from the recordings of shotpoints 28, 36, and 29. Amplitudes are plotted true after correcting for spherical divergence and bandpass filtering between 10-45 Hz. The figure indicates the quality of the data and some of the main characteristics of the Colorado Plateau/Basin and Range Transition. Based on the reflection data and for purposes of discussion, the crust is described in terms of four units, an upper, middle, lower crust, and upper mantle. The upper crust (< 4 s two-way travel time (TWTT)) displays prominent reflectors throughout, the most conspicuous being the "Bagdad Reflectors" discussed by *Goodwin et al.* [1989]. The middle crust, between 4.0-6.0 s, is transparent seismically. The top of the lower crust is marked by the onset of reflectivity, beginning at ≈5.8 s and 2 km and increasing to ≈6.8 s TWTT at 20 km. The entire lower crust is highly reflectivity. The reflector "R"", when used as a reference mark, indicates roughly 3 km of crustal thickening in the direction of the Colorado Plateau. A prominent Moho

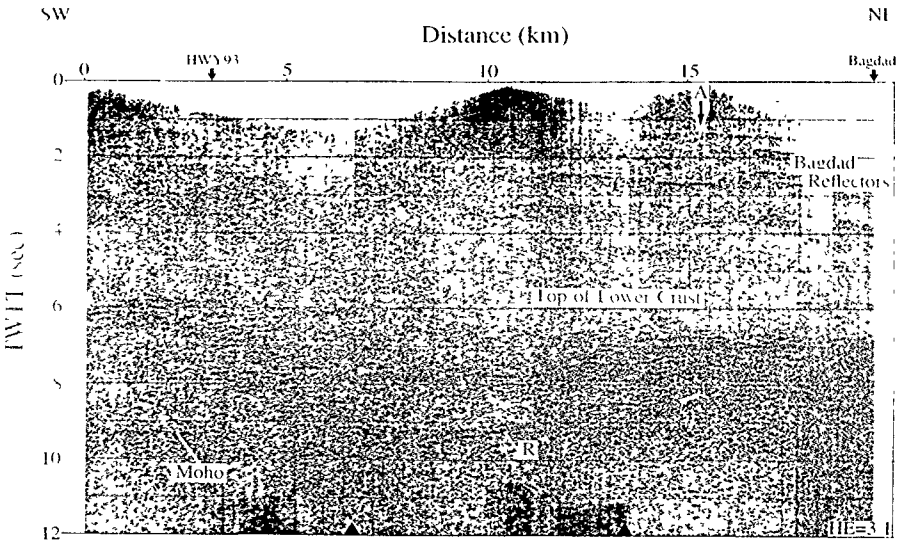

Figure 3. Single-fold reflection data recorded from SP28, 29, and 36. See Figure 1 for location. Data corrected for spherical divergence and bandpass filtered between 10-45 Hz. Triangles at bottom of section separate that data from SP28, 36, and 29. Horizontal exaggeration is approximately 3:1 at 6.0 km s^{-1}.

reflection is missing from these data, but some hint of it is seen at ≈9.2 s and 2.5 km. Below ≈10 s, the upper-mantle appears transparent as reflectivity diminishes. The top and bottom the zone of lower crustal reflectivity is in agreement with the results of *McCarthy et al.* [1990].

5. Finite Element Synthetic Seismograms

Explicit second or fourth order finite element/finite difference methods have been used in a variety of geophysical applications that range from relatively low frequency strong ground motion modeling [*Vidale et al.*, 1985] to high frequency reverse time migration of seismic reflection data [*Chang and McMechan*, 1987]. The success of the method is primarily due to its ability to accurately compute full wavefield synthetic seismograms for arbitrarily complex velocity structures and complex sources. This ability to model complex velocity structure has found an application in the simulation and modeling of seismic coda observed in reflection/refraction data [*Gibson and Levander*, 1988], regional surface waves [*Jih and McLaughlin*, 1988], earthquake data [*Frankel and Clayton*, 1984], and teleseisms [*McLaughlin*, 1986] using models of random velocity variation.

In this study, we will use the traditional Galerkin formulation of the finite element method [*Zienkiewicz*, 1983], a formulation implemented by *Wojcik et al.* [1988]. The finite element synthetic seismograms have not been used as extensively as finite difference techniques, but has been particularly successful in earthquake source studies [*McGowan et al.*, 1977; *Archuleta and Day* , 1980; *Geller et al.*, 1979; *Archuleta and Frazier* , 1978]. Both the finite element and finite difference method belong to a general class of methods known as the method of weighted residuals [*Huebner and Thornton*, 1982]. Unlike the finite difference method, the finite element method does not define the velocity and density model as a set of discrete grid points, but as an assemblage of piece-wise continuous subdomains or elements, over which the displacement is defined by an approximating polynomial [*Zienkiewicz*, 1983]. Reduced to a linear system of second order ordinary differential equations, the displacements at the elemental nodes are calculated from the displacements at the previous two time-steps and the displacements at the surrounding nodes. A

lucid discussion on the formulation and error analysis of the finite element and finite difference techniques can be found in *Marfurt* [1985].

6. Realization of a Random Velocity Structure

An important aspect in synthetic seismogram modeling of crustal scattering is the accurate statistical description of the random velocity structure. While much work has been done on quantifying the size and strength of random scatterers in the crust [*Frankel and Clayton*, 1984; *Gibson and Levander*, 1988], only a limited number of data sets have been investigated. Therefore, fundamental concepts on the scale length and strength of crustal scattering for different geological provinces are not well known. Thus far, modeling studies have typically used either gaussian, exponential, or self-similar correlation functions [*Frankel and Clayton*, 1984; *Gibson and Levander*, 1988; *Jih and McLaughlin*, 1988] to generate realizations of the velocity field.

Figure 4a shows an isotropic random field that is typically incorporated as the stochastic component of the velocity model. In this example, an exponential correlation function, with a correlation length of 200 m, was used to generate the random field. While isotropic correlation functions have been successful in numerical studies of seismic coda, they may not always be appropriate. This is particularly true in the Basin and Range, where active extension since Cenozoic time has produced a sub-horizontal crustal fabric. Conventional CDP reflection profiling across the Basin and Range [*Allmendinger et al.*, 1987; *Klemperer et al.*, 1986; *Hague et al.*, 1987] and individual shot gathers (Fig. 3) are in accord with the view of pervasive lower crustal reflectivity that is dominated by a sub-horizontal reflection pattern. Such patterns are probably produced by thermal and rheologic processes that have preferentially deformed the ductile lower crust in the direction of maximum extension. While conventional CMP processing of deep crustal reflections may produce the appearance of sub-horizontal reflectivity [*Gibson and Levander*, 1988], it is difficult to argue that sub-horizontal lower crust fabric do not significantly contribute, given the recent tectonic evolution of the Basin and Range.

EXPONENTIAL RANDOM MEDIA

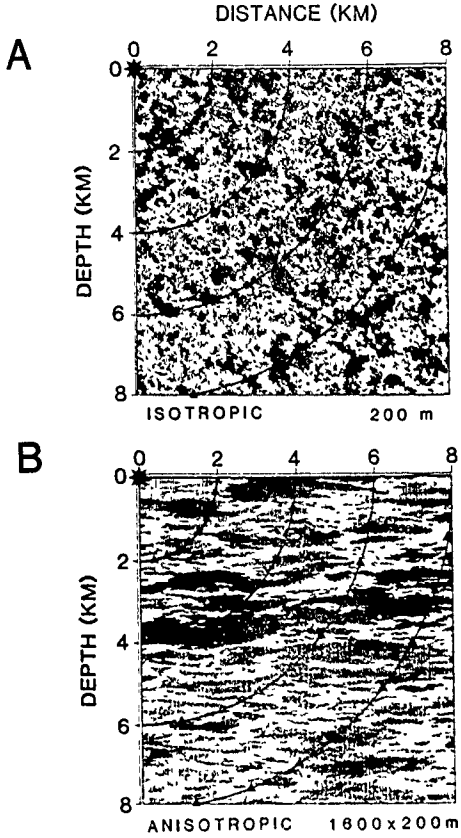

Figure 4. Two-dimensional realizations of (a) an exponential isotropic random media with a horizontal and vertical correlation length of 200 m and (b) an exponential anisotropic random media with a horizontal and vertical correlation length of 1600 m and 200 m, respectively. The light and dark regions represent high and low velocities about a mean background velocity.

An alternative model to the isotropic random media is a realization using an anisotropic correlation function, where the spatial lag differs between the horizontal and vertical directions. Shown in Figure 4b is an anisotropic random media where the horizontal and vertical correlation lengths are 1600 m and 200 m, respectively. We feel this model represents a compromise between the velocity structure used by *Gibson and Levander* [1989] to model the Rhine graben refraction data and the one-dimensional plane layer model of *Sandmeier et al.* [1987]. It also approximates a sub-horizontal fabric that might be representative, in a generic way, of the lower crust in the Basin and Range.

7. Finite Element Simulations of the 1987 PACE Seismic Data

Wide-angle Refraction Data from SP21

To investigate the effects that different random media have on wave propagation, we will compared observed seismic refraction data (SP21) with two-dimensional synthetic seismogram simulations that incorporate random velocity variation in the lower crust. The deterministic two-dimensional velocity structure used as a basis was derived from iterative travel time modeling [*McCarthy et al.*, 1990]. The three synthetic seismogram record sections presented were calculated from: 1) a finite element grid derived from the velocity model of *McCarthy et al.* [1990]; 2) a lower crust velocity model with isotropic small-scale heterogeneities, similar to that in Figure 4a; and 3) a lower crustal velocity model with anisotropic small-scale heterogeneities, similar to that in Figure 4b.

Figure 5 shows the two-dimensional velocity structure [*McCarthy et al.*, 1990] used in the three finite element simulations. The two-dimensional finite element velocity model was constructed by digitizing the raytrace model (Fig. 5) every 43 m. To avoid prohibitively long run times due to low sediment velocities, P-wave velocities less than 6.0 km s^{-1} were reset to a velocity of 6.0 km s^{-1}. This enabled the calculation of high frequency synthetic seismograms, given a 43 m nodal spacing, but eliminated the effects of near-surface sedimentary structure in the calculations. S-wave velocities were scaled relative to the P-wave velocities assuming a Poisson's ratio of 0.25 and

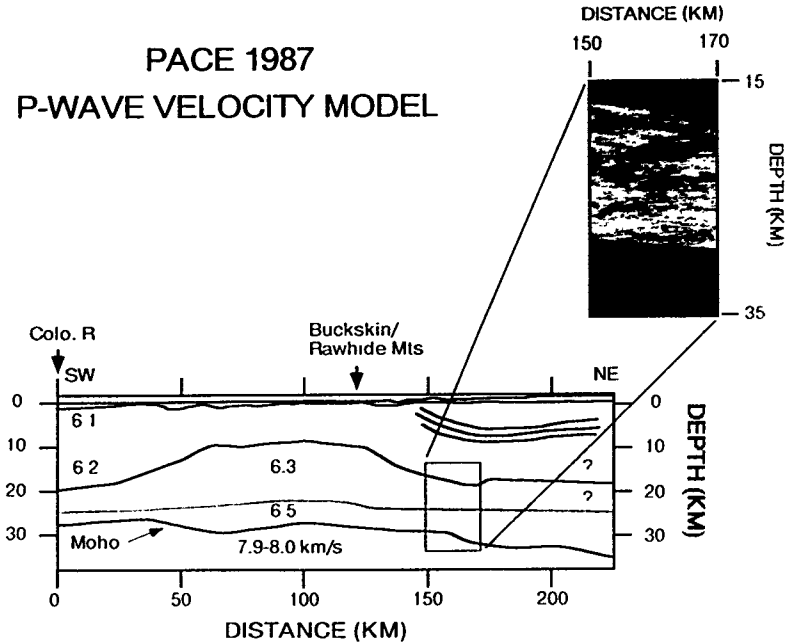

Figure 5. Two-dimensional velocity-depth structure derived from travel time and amplitude modeling of the 1987 PACE refraction data [*McCarthy et al.*, 1990].

densities were calculated using the empirical relationship $\rho = 0.252+0.3977\alpha$ [*Nafe and Drake*, 1957], where ρ is the density and α is the P-wave velocity.

The left side of the finite element grid is located at SP21 and is modeled as a plane of symmetry. The bottom and right edges of the grid are A2 absorbing boundaries [*Clayton and Engquist* , 1977] and the top of the grid is a stress-free boundary. The finite element model was 180 km in length and 37 km in depth. The source is an isotropic line source and the source-time function is a Ricker wavelet with a half-power frequency of 8.0 Hz, resulting in approximately 17 nodes per wavelength for the slowest P-wave and 10 nodes per wavelength for the slowest S-wave. The finite element formulation assumes a purely elastic model, hence, intrinsic attenuation is not accounted for in the calculations.

Figure 6 shows a comparison of the observed refraction section and the finite element synthetic seismograms for a deterministic medium. The comparison shows that the relative travel time and amplitude of the major crustal P-wave phases are well modeled by the finite element synthetic seismograms. The existence of significant pre-critical PmP energy in the synthetic seismograms suggests that the model's crust-mantle transition is too sharp and that a transitional Moho is more appropriate [*Braile and Smith*, 1977]. For offsets greater than 60 km, Pg is over-predicted relative to the observed data. In general, the Basin and Range exhibits low upper crustal Q (<200-300; *Braile*, 1977; *Benz et al.*, 1990), which causes noticeable amplitude and frequency loss for offsets greater than 60 km. Since the finite element simulations assume purely elastic media, intrinsic attenuation cannot be accounted for and the resulting synthetics over-predict the Pg and PiP amplitudes at larger offsets.

Isotropic Random Medium—In this simulation, an isotropic, exponential random velocity structure was incorporated into the lower crust. The random medium is similar to that seen in Figure 4a. The random medium was generated with a correlation length of 200 m and a 5% standard deviation (std) relative to an average lower crustal background velocity of 6.5 km s^{-1}. Shown in Figure 7 is a comparison of the observed and theoretical seismograms. It can be seen that the scattering effects from this model are

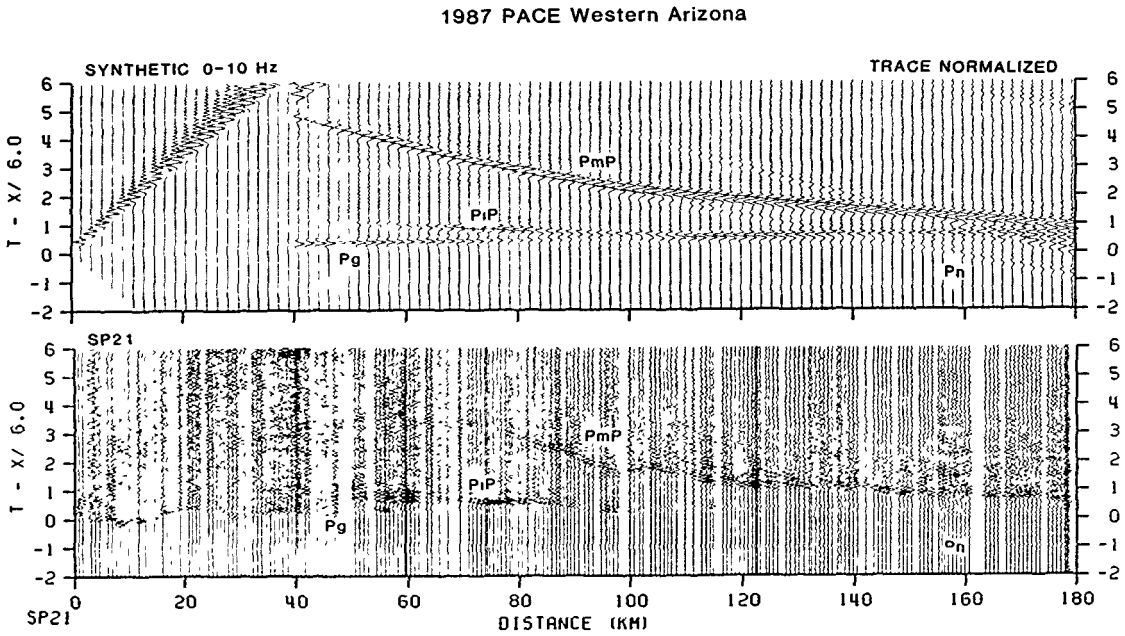

Figure 6. Comparison of trace normalized refraction data (SP21) and finite element synthetic seismograms computed for the two-dimensional velocity model shown in Figure 4 but without scatterers.

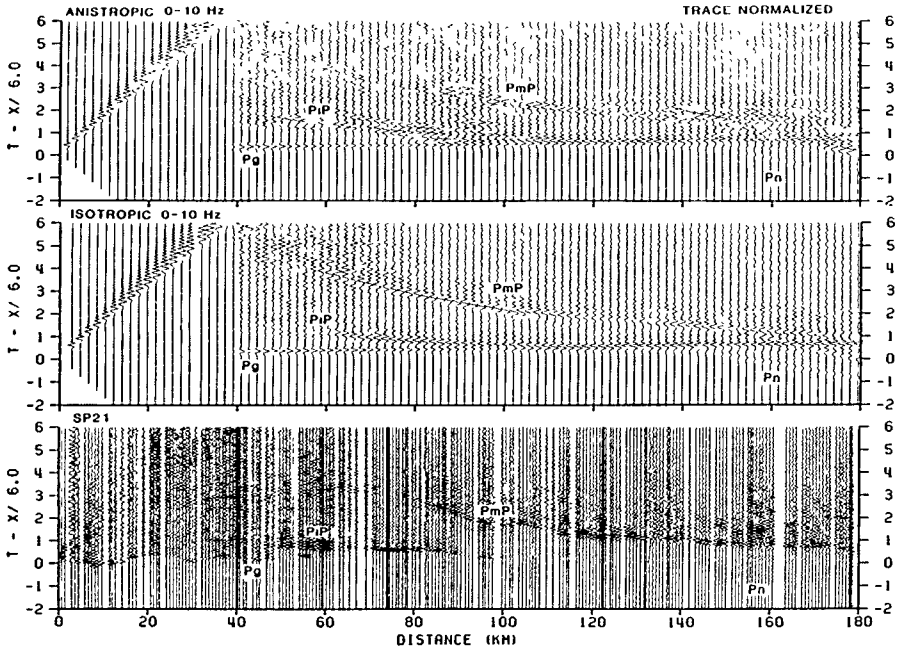

Figure 7. Comparison of trace normalized refraction data (SP21) and finite element synthetic seismograms, a) anisotropic random velocities in the lower crust, b) isotropic random velocities in the lower crust. The random medium has a 5% standard deviation (std) about a mean lower crustal velocity of 6.5 km s^{-1}. For the anisotropic case the horizontal and vertical correlation lengths are 1600 and 200 m, respectively, and 200 m for the isotropic case.

noticeable as coda following the PiP and PmP phases The largest difference between this simulation and the previous one is the loss of correlatable pre-critical PmP energy for distances less than 60 km. This simulation suggests that a transitional Moho is not required to explain the lack of pre-critical PmP energy in the observed data. Results show that lower crustal velocity fluctuations distort the amplitude and phase of the relatively weak, precritical PmP, giving it the appearance of a transitional Moho. Beyond the critical point, the amplitude of the PmP increases such that coherency is maintained with offset but noticeable amplitude decay occurs. This is due to significant P-to-P and P-to-S conversions that effectively partition energy away from the direct wave, in this case the PmP phase. Possibly, the standard deviation of the random velocity structure is too large and the consequence is significant amplitude loss of PmP.

Anisotropic Random Media—In this simulation, an anisotropic, exponential, random velocity structure, similar to that shown in Figure 4b, is incorporated into the lower crust. The horizontal and vertical correlation lengths are 1600 m and 200 m, respectively. Like the previous simulation, the random fluctuations in velocity have a 5% std relative to an average lower crustal background velocity of 6.5 km s^{-1}. The observed and theoretical seismograms for this simulation are shown in Figure 7. When compared to the previous simulation, the synthetic seismograms in Figure 7 show quite a difference in both the character of the coda and in the amplitude variations of the PiP and PmP phase. The coda following PiP and PmP display significant coherency that appears as prominent phases that can be correlated up to 20 km. The best example of this is the phase that follows closely in time PiP between 60 and 90 km. These coherent and relative large coda waves have the effect of decreasing the coherency of the principal body waves, both PiP and PmP. Similar to the previous simulation, the precritical PmP reflection is weak and incoherent.

When compared to the observed data, the synthetic seismograms replicate some of the complexity of the data. The majority of coda is seen as wide-angle P-to-P conversions, which produced the relatively large coherent coda. Correlatable coda energy is observed as phases that cannot by described and modeled in conventional terms, like Pg, PiP, and PmP. For example, between

80-100 km, weak coherent energy precedes PmP by ~0.5-1.0 s reduced time. In addition, an enechelon pattern of energy is observed to follow the PmP for ≈2.0 s, which is similar to that found in the synthetic seismograms. Unlike the observed data, the synthetic seismograms predict a PmP phase that is not as coherent between 80-180 km as that observed. This observation demonstrates the sensitivity of the incident wave to the correlation length of the scattering media and possibly the size of the velocity fluctuations. Perhaps, had the aspect ratio or standard deviation been smaller, the simulations may have predicted a higher degree of coherency for the PmP phase.

These simulations demonstrate that certain aspects of each model fit the observed data. The isotropic random media predicts more coherency of PmP, but less coherency of the coda. By way of contrast, the anisotropic random media predict coherency in the coda and less coherency of PmP. Both these results can be explained in terms of the types of body waves scattered from the incident wavefield. In an isotropic random medium, for all angles of incidence, the incident wavefield will produce scattered P and S energy. Because the dimensions of the scattering body are close to that of the incident wavefield, scattering occurs over a wide range of angles and, therefore, no coherent wide-angle coda is produced. For the anisotropic random media, the strongest scattering will occur over a restricted range of incident angles, which correspond to wide-angle P-to-P conversion. This process produces the coherent wide-angle P-wave coda that has an apparent velocity similar to PmP.

These results represent only a limited number of simulations, so only general comments can be made about lower crustal structure. This synthetic seismograms for the isotropic case suggest that 5% std is too large, since PmP cannot propagate to large distances due to effective P-to-P and P-to-S scattering, which rapidly partitions energy away from PmP. The anisotropic case also indicates that 5% std is possibly too large, because the amplitudes of the wide-angle P-wave coda are over predicted, compared to PmP. It is also possible that the aspect ratio for the anisotropic case is too large, considering that the synthetic seismograms predict coherent P-wave coda over distances ranges of 30 km, which is larger than that seen in the data. At this point, not enough simulations have been done for a range of velocity models to

determine what is the range of permissible structures that predict the observed data.

8. Near-Vertical Reflection Data from SP28

Near-vertical synthetic seismograms have been calculated to understand the near-vertical response of the two random media investigated in the previous section. The simulations are computed using a velocity structure constructed by digitized the two-dimensional velocity (Fig. 5) every 5 m starting near SP28. The finite element model has a length of 20 km and depth of 40 km. Peak frequency of the Ricker source wavelet is 20 Hz. Based on the calculations in the previous section, it is assumed that a 5% std is too large, and the following simulations assume a 3% std about a mean lower crustal velocity of 6.5 km s^{-1}. Figure 8 shows examples of the velocity-depth function selected from one location (SP28). Figure 8a is the velocity-depth function assuming no random distribution of velocity in the lower crust, while Figure 8b is the velocity-depth function assuming random variations of velocity in the lower crust. In addition, synthetic seismograms are also calculated for a model with a transitional crust-mantle boundary (Fig. 8c). A transitional crust-mantle boundary is investigated since the lower-frequency wide-angle synthetic seismograms (Fig. 7) argued against a transitional Moho, based on the lack of coherent pre-critical PmP energy. These same wide-angle synthetic seismograms contradicted the results from the model with smoothly-varying lower crustal velocities (Fig. 6) and, therefore, proved inconclusive about the transitional nature of the Moho.

The near-vertical synthetic seismograms for the different cases is shown in Figure 9. The single-fold shot gathers are corrected for spherical divergence and plotted relative true amplitude. The synthetic seismograms for the isotropic and anisotropic random media and 1st order Moho show that the most prominent phase is the PmP reflection (≈9.5 s TWTT). As expected, the anisotropic case predicts a greater degree of sub-horizontal reflectivity. For the isotropic case, the coda is longer in duration and is seen as the reflectivity arriving after the PmP reflection (>9.5 s TWTT). Over a wide-range of incidence angles, isotropic random media will produce both P-to-P and P-to-S scattering, relative to an incident P-wave. Since the travel time of back-

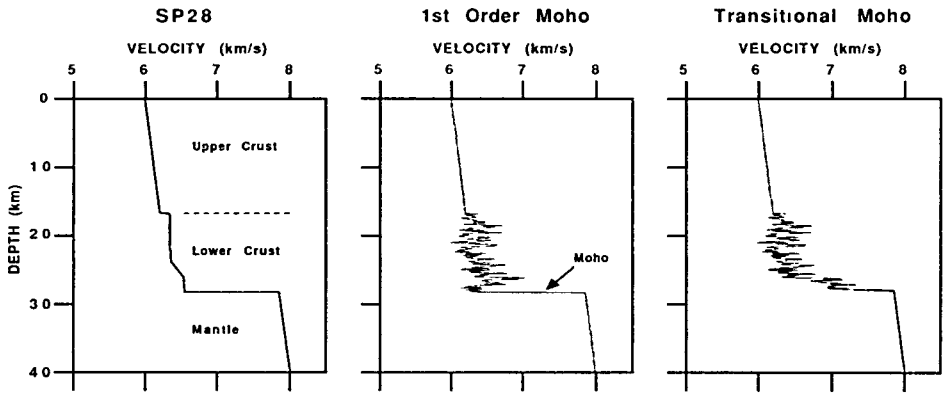

Figure 8. One-dimensional velocity-depth functions at SP28 showing, a) the velocity-depth structure of McCarthy et al. [1990], b) a random velocity structure in the lower crust and 1st order Moho, and c) a random velocity structure and transitional Moho. The velocity perturbation is 3% about a mean background velocity of 6.5 km s^{-1}.

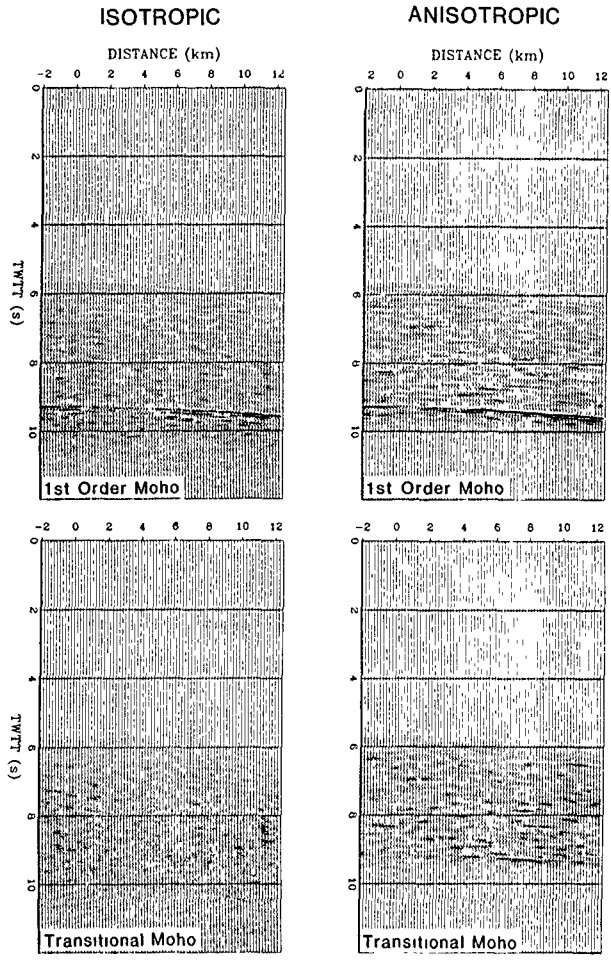

Figure 9. Finite element synthetic seismograms for SP28. The two-dimensional velocity model included isotropic and anisotropic random media in the lower crust. The random media is 3% std about a mean lower crustal velocity of 6.5 km s^{-1} Source-time function is a Ricker wavelet with a peak frequency of 12 Hz.

scattered S-waves are longer, the corresponding coda will be longer. This contrasts with the anisotropic case, which is dominated by P-to-P scattering, due to the steep incidence angles and sub-horizontal fabric. The coda is mostly back-scattered P-wave energy with travel times closer to the incident P-wave and, subsequently, shorter coda durations. Synthetic seismograms for the transitional Moho models are similar to the previous simulations except of the lack of a prominent PmP reflection, which is in agreement with the observed data (Fig 3). Based on a qualitative comparisons, the synthetic seismograms for the anisotropic random media and transitional Moho appear to best fit the observed near-vertical reflection data (Fig. 3).

9. Discussion and Conclusions

Composition From Seismic Velocity Models—The P-wave crustal structure derived here provides constraints on the composition and structure of the upper lithosphere. To place constraints on crustal composition in the southern Basin and Range, we show plausible rock types, taken from the laboratory measurements of seismic velocities by *Christensen* [1979] and plotted relative to the generalized velocity-depth function (Fig. 10A). The laboratory determined velocities are corrected for temperature assuming a regional surficial heat flow of 90 mW m^{-2} and pressure effects assuming a mean crustal density of 2.8 g cm^{-3}. The crustal geotherm used to correct the laboratory velocities is shown in Figure 11B.

The important observation (Fig. 10A) is that no one rock type follows the interpreted velocity-depth model for more than a few kilometers. We have chosen only a small number of rock compositions and metamorphic grades from *Christensen* [1979], but we feel these reflect a representative sampling of plausible rock types. We assume that granulite-grade metamorphism is achieved in the lower crust of the Basin and Range due to the high pressures (900 GPa) and temperatures (>900°C). Based on these observations, the upper crust appears to best fit a general suite of granitic-dioritic to quartz-rich granulitic rocks (5.5 to 6.2 km s^{-1}), while amphibolite to mafic granulites fit the lower crust, 6.4 to 6.8 km s^{-1}. The correlations imply that the bulk crustal composition varies with depth, but the correlation of velocity with composition is non-unique. The primary difficulty arises from the fact that

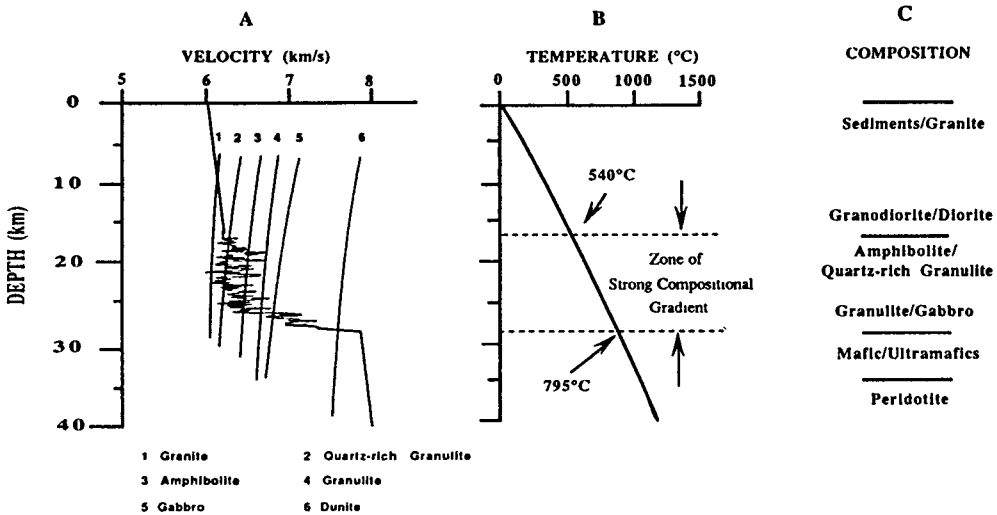

Figure 10. Generalized seismic velocity, temperature, and composition in northern Arizona. Predicted velocity-depth function of plausible continental crust and upper-mantle rock types and metamorphic grades are superimposed on the generalized velocity-depth function. The compositions, metamorphic grades, temperature, and pressure coefficients were taken from Christensen [1979]. Temperature and pressure corrections with depth were made assuming a 90 mW m^{-2} surface heat flow and a mean crustal density of 2.67 g cm^{-3}.

the lower crust has a seismic velocity gradient that is difficult to constrain, but likely ranges from 0.02 to 0.04 s^{-1}, whereas most rock samples exhibit weak pressure derivatives (0.002 s^{-1} or less; *Christensen*, 1979) at pressures appropriate for the lower crust. Furthermore, the high lower-crustal temperatures in this region of high heat flow should further decrease the velocity gradient at depth [*Christensen*, 1979]. A 3% std in velocity for the lower crust tend to bracket the range of crustal compositions, implying that the lower crust may consist of a large compositional suite. This observation is in agreement with laboratory studies of exposed portions of the lower crust that show large variations in velocity and composition [*Fountain*, 1976].

Wide-angle Elastic Wave Propagation in Random Media—These simulations have clearly demonstrated that elastic waves are sensitive to the type of random media, when viewed over a wide-ranges of incidence angles. The incidence wave and coda behave differently to differences in the random media, e. g. isotropic versus anisotropic small-scale heterogeneities. Further understanding of elastic wave scattering in the crust requires high resolution recordings of seismic data at near-vertical to wide-angles. Coherency analysis of both the direct wave (e.g. the PmP phase) and coda, as a function of offset and frequency, are necessary to constrain possible models of small-scale velocity heterogeneities. Furthermore, a comprehensive understand of crustal scale-lengths and attenuation requires a better understanding of the differences observed in both the back-scattered P- and S-wavefields. Investigations of crustal scattering have important implications over a broad range of seismic applications, these include: 1) understanding the generation and propagation of regional phases used in the location, discrimination, and yield estimation of nuclear explosions; 2) determining the bulk properties of the crust, based on composition and velocity relationships; 3) understanding and differentiating the role of scattering and intrinsic attenuation in the crust, which has implications concerning the crust's physical state.

Acknowledgements

Discussions with W. Mooney, G. Randall, and A. Frankel provided new insights into the topic of the paper. Reviews by W. Mooney and J. McCarthy of the USGS greatly improved the paper. The USGS and Stanford provided support for the field experiment and field recorders. We thank A. Tompson of Lawrence Livermore National Laboratory for use of his "turning bands" program for generating two-dimensional random medium.

References

Allmendinger, R. W., J. W. Sharp, D. V. Tish, L. Serpa, L. Brown, S. Kaufman, J. Oliver, and R. B. Smith, Cenozoic and Mesozoic structure of the eastern Basin and Range province, Utah from COCORP seismic reflection data, *Geology, 11*, 532-536, 1983.

Allmendinger, R. W., T. A. Hauge, E. C. Hauser, C. J. Potter, S. L. Klemperer, K. D. Nelson, P. Knuepfer, J. Oliver, Overview of the COCORP 40° N Transect, western United States: The fabric of an orogenic belt, *Geol Soc. Am. Bull., 98*, 308-319, 1987.

Archuleta, R. J., and G. A. Frazier, Three-dimensional numerical simulations of dynamic faults in a half-space, *Bull. Seism. Soc. Am., 68*, 541-572, 1978.

Archuleta, R. J., and S. M. Day, Dynamic rupture in a layered medium: The 1966 Parkfield earthquake, *Bull Seism. Soc. Am., 70*, 671-689, 1980.

Atwater, T., Implications of plate tectonics for the Cenozoic tectonic evolution of western North America, *Geol. Soc Am. Bull., 81*, 3513-3535, 1970.

Benz, H. M., R. B. Smith, W. D. Mooney, Crustal structure of the northwestern Basin and Range province from the 1986 PASSCAL seismic experiment, J. Geophys. Res., 1990 (in press).

Bird, J. M., and J. F. Dewey, Lithosphere plate-continental margin tectonic, *Geol. Soc. Am. Bull., 81*, 1031-1059, 1970.

Blackwell, D. O., Heat flow and energy loss in the western United States, in *Cenozoic Tectonics and Regional Geophysics of the Western Cordillera*, edited by R. B. Smith and G. P. Eaton, *Geol. Soc. Am. Memoir 152*, 175-208, 1978.

Braile, L. W., Interpretation of crustal velocity gradients and Q structure using amplitude-corrected seismic refraction profiles, in *The Earth's Crust, Am. Geophys. Union Mono. 20*, 427-439, 1977.

Cerveny, V., M. M. Popov, and I. Psencik, Computation of wave fields in inhomogeneous media-Gaussian beam approach, *Geophys. J. R. Astr. Soc.*, *70*, 109-128, 1982.

Chang, W., and G. A. McMechan, Elastic reverse-time migration, *Geophysics, 52*, 1365-1375, 1987.

Christensen, N. I., Compressional wave velocities in rocks at high temperatures and pressures, critical thermal gradients, and crustal low-velocity zones, *J. Geophys. Res., 84*, 6849-6857, 1979.

Clayton, R. W., and B. Engquist, Absorbing boundary conditions for acoustic and elastic wave equations, *Bull. Seism. Soc. Am., 67*, 1529-1540, 1977.

Coney, P. J., and T. A. Harms, Cordilleran metamorphic core complexes: Cenozoic extensional relics of Mesozoic compression, *Geology, 12*, 550-554, 1984.

Eaton, J. P., Crustal structure from San Francisco, California to Eureka, Nevada, from seismic refraction measurements, *J. Geophys. Res., 68*, 5789-5806, 1963.

Eaton, G. P., Regional geophysics, Cenozoic tectonics, and geologic resources of the Basin and Range province and adjoining regions, in *Basin and Range Symposium*, edited by G. W. Newman and H. D. Goode, *Rocky Mountain Assoc. of Geol. 1979 Symposium*, 11-39, 1979.

Eddington, P.J., R. B. Smith, and C. Renggli, Kinematics of Basin-Range intraplate extension, eds. Coward, M.P., Dewey, J.F., and Hancock, P.L., in *Continental Extension, London Geological Soc., Special Publication 28*, 371-392, 1987.

Frankel, A., and R. W. Clayton, A finite difference simulation of wave propagation through random media, *Bull. Seism. Soc. Am.*, *74*, 2167-2186, 1984.

Fountain, D. M., The Ivrea-Verbano and Strona Ceneri zones, northern Italy: A cross section of the continental crust; New evidence from seismic velocities, *Tectonophysics, 33*, 145-165, 1976.

Gibson, B. S., and Levander, A. R. (1988). Modeling and processing of scattered waves in seismic reflection surveys, *Geophysics, 53*, 466-478.

Gajewski, D., and C. Prodehl, Seismic refraction investigation of the Black Forest, *Tectonophysics, 142*, 27-48, 1987.

Goodwin, E. B., and J. McCarthy, Composition of the lower crust in west-central Arizona from three-component seismic data, *J. Geophys. Res.*, 1990 (in press).

Hague, T. A., R. W. Allmendinger, C. Caruso, E. C. Hauser, S. L. Klemperer, S. Opdyke, C. J. Potter, W. Sanford, L. Brown, S. Kaufman, and J. Oliver, Crustal structure of western Nevada from COCORP deep seismic-reflection data, *Geol. Soc. Am. Bull.*, *98*, 320-329, 1987.

Healy, J. H., W. D. Mooney, H. R. Blank, M.E. Gettings, W. M. Kohler, R. J. Lamson, and L. E. Leone, Saudi Arabian seismic deep-refraction profile: final project report, *U. S. Geol. Surv. Open-File Rept. USGS-OF-02-37*, 429 pp., 1982

Hill, D. P., and L. C. Pakiser, Crustal structure between the Nevada Test Site and Boise, Idaho, from seismic refraction measurements, in *The Earth beneath the Continents*, edited by J. S. Steinhart and T. J. Smith, *Am. Geophys. Union Mon.10*, 391-419, 1966.

Huebner, K. H., and E. A. Thornton (1982). *The Finite Element Method for Engineers*, John Wiley and Sons, New York, 623p.

Klemperer, S. L., T. A. Hauge, E. C. Hauser, J. E. Oliver, and C. J. Potter, The Moho in the northern Basin and Range province, Nevada, along the COCORP 40° N seismic reflection transect, *Geol. Soc. Am. Bull., 97*, 603-618, 1986.

Kohler, W. M., GRID, Version 1.20: A computer program for calculation of time terms using seismic travel times, *U.S. Geol Surv. Open-File Rept 88-671*, 39 p., 1988.

Lachenbruch, A. H., and J. H. Sass, Models of an extending lithosphere and heat flow in the Basin and Range province, in *Cenozoic Tectonics and Regional Geophysics of the Western Cordillera*, edited by R. B. Smith and G. P. Eaton, *Geol. Soc. Am. Memoir 152*, 209-250, 1978.

Larkin, S. P., J. McCarthy, and G.S. Fuis (1988). Data report for the PACE 1987 seismic refraction survey, west-central Arizona, *U.S. Geol. Surv. Open-File Rept.*

Marfurt, K. J., Accuracy of finite-difference and finite-element modeling of the scalar and elastic wave equations, *Geophysics, 49*, 533-549, 1984.

McCarthy, J., S. P. Larkin, G. S. Fuis, and R. Simpson, Anatomy of a metamorphic core complex: Seismic refraction and wide-angle reflection profiling in southeastern California and western Arizona, *J. Geophys. Res.*, submitted, 1990.

McGowan, D. W., P. Glover, and S. S. Alexander, A static and dynamic finite element analysis of the 1971 San Fernando, California, earthquake, *Geophys. J. R. Astron. Soc., 48*, 163-185, 1977.

Mooney, W. D., and L. W. Braile, The seismic structure of the continental crust and upper mantle of North America, in *The Geology of North America--An overview*, edited by A. W. Bally and A. R. Palmer, *Geol Soc. Am.*, 39-52, 1989.

Nafe, J.E., and C. L. Drake, Variations with depth in shallow and deep water marine sediments of porosity, density, and the velocities of compressional and shear waves, *Geophysics, 22*, 523-552, 1957.

Pakiser, L. C., Structure of the crust and upper mantle in the western United States, *J. Geophys. Res., 68*, 5747-5756, 1963.

Pakiser, L. C., Geophysics of the intermontane system, in *Geophysical Framework of the Continental United States*, edited by L.C. Pakiser and W.D. Mooney, *Geol. Soc. Am. Memoir 172*, 235-247, 1989.

Priestley, K. F., A. S. Ryall, and G. S. Fezie, Crust and upper-mantle structure in the northwest Basin and Range province, *Bull. Seism. Soc. Am., 72*, 911-923, 1982.

Prodehl, C., Crustal structure of the western United States, *U. S. Geol. Surv. Prof. Pap.,1034,* 74 pp., 1979.

Roller, J. C., Crustal structure in the eastern Colorado Plateaus province from seismic-refraction measurements, *Bull. Seism. Soc. Am., 55*, 107-119, 1965.

Sandmeier, K.J., W. Walde, and F. Wenzel, Physical properties and structure of the lower crust revealed by one and two-dimensional modeling, *Geophys. J. R. Astr. Soc., 89*, 339-344, 1987.

Smith, R. B., Seismicity, crustal structure and intraplate tectonics of the interior of the western Cordillera, in *Cenozoic Tectonics and Regional Geophysics of the Western Cordillera*, edited by R. B. Smith and G. P. Eaton, *Geol. Soc Am. Memoir 152*, 111-144, 1978.

Smith, R.B., W.C. Nagy, K.A., Julander, J.J., Viveiros, C.A., Barker, and D.G. Gants, Geophysical and Tectonic Framework: Basin-Range to Colorado Plateau-Rocky Mountain Transition, in *Geophysical Framework of the Continental United States*, edited by L.C. Pakiser and W.D. Mooney, *Geol Soc. Am. Memoir 172*, 205-233, 1989.

Speed, R. C., Evolution of the sialic margin in the central western United States, In *Geology of Continental Margins*, edited by J. Watkins and C. Drake, *Am. Assoc. of Petrol. Geol., 34*, 452-468, 1982.

Stauber, D. A., and D. M. Boore, Crustal thickness in northern Nevada from seismic refraction profiles, *Bull. Seism. Soc. Am., 68*, 1049-1058, 1978.

Thompson, G. A., and D. B. Burke, Regional geophysics of the Basin and Range province, *Annu. Rev. Earth and Planet. Sci., 2*, 213-238, 1974.

Thompson, G. A., R. Catchings, E. Goodwin, S. Holbrook, C. Jarchow, C. Mann, J. McCarthy, and D. Okaya, Geophysics of the western Basin and Range province,in *Geophysical Framework of the Continental United States.*, edited by L.C. Pakiser and W. D. Mooney, *Geol. Soc. Am. Memoir 172*, 177-203, 1989.

Wright, L., Late Cenozoic fault patterns and stress fields in the Great Basin and westward displacement of the Sierra Nevada block, *Geology, 4*, 489-494, 1976.

Wojcik, G. L., D. K. Vaughn, M. Barenberg, J. Mould, and M. B. Hulit, Large-scale, explicit wave simulations on the Cray-2, *Appl. Num. Math.*, 1988.

Vidale, J., D. V. Helmberger, and R. W. Clayton, Finite-difference seismograms for SH waves, *Bull. Seism. Soc. Am., 75*, 1765-1782, 1985.

Zienkiewicz, O. C. (1983). *The Finite Element Method*, McGraw-Hill, London, 797p.

Prof Thomas Ahrens
Seismological Lab, 252-21
Division of Geological & Planetary Sciences
California Institute of Technology
Pasadena, CA 91125

Prof. Charles B. Archambeau
CIRES
University of Colorado
Boulder, CO 80309

Dr. Thomas C. Bache, Jr.
Science Applications Int'l Corp
10260 Campus Point Drive
San Diego, CA 92121 (2 copies)

Prof. Muawia Barazangi
Institute for the Study of the Continent
Cornell University
Ithaca, NY 14853

Dr Douglas R. Baumgardt
ENSCO, Inc
5400 Port Royal Road
Springfield, VA 22151-2388

Prof Jonathan Berger
IGPP, A-025
Scripps Institution of Oceanography
University of California, San Diego
La Jolla, CA 92093

Dr Lawrence J. Burdick
Woodward-Clyde Consultants
566 El Dorado Street
Pasadena, CA 91109-3245

Dr. Jerry Carter
Center for Seismic Studies
1300 North 17th St., Suite 1450
Arlington, VA 22209-2308

Dr. Karl Coyner
New England Research, Inc
76 Olcott Drive
White River Junction, VT 05001

Prof. Vernon F. Cormier
Department of Geology & Geophysics
U-45, Room 207
The University of Connecticut
Storrs, CT 06268

Professor Anton W. Dainty
Earth Resources Laboratory
Massachusetts Institute of Technology
42 Carleton Street
Cambridge, MA 02142

Prof. Steven Day
Department of Geological Sciences
San Diego State University
San Diego, CA 92182

Dr. Zoltan A. Der
ENSCO, Inc
5400 Port Royal Road
Springfield, VA 22151-2388

Prof. John Ferguson
Center for Lithospheric Studies
The University of Texas at Dallas
P.O. Box 830688
Richardson, TX 75083-0688

Dr. Mark D. Fisk
Mission Research Corporation
735 State Street
P. O. Drawer 719
Santa Barbara, CA 93102

Prof. Stanley Flatte
Applied Sciences Building
University of California
Santa Cruz, CA 95064

Dr. Alexander Florence
SRI International
333 Ravenswood Avenue
Menlo Park, CA 94025-3493

Prof. Henry L. Gray
Vice Provost and Dean
Department of Statistical Sciences
Southern Methodist University
Dallas, TX 75275

Dr. Indra Gupta
Teledyne Geotech
314 Montgomery Street
Alexandria, VA 22314

Prof. David G. Harkrider
Seismological Laboratory
Division of Geological & Planetary Sciences
California Institute of Technology
Pasadena, CA 91125

Prof Donald V. Helmberger
Seismological Laboratory
Division of Geological & Planetary Sciences
California Institute of Technology
Pasadena, CA 91125

Prof. Eugene Herrin
Institute for the Study of Earth and Man
Geophysical Laboratory
Southern Methodist University
Dallas, TX 75275

Prof. Bryan Isacks
Cornell University
Department of Geological Sciences
SNEE Hall
Ithaca, NY 14850

Dr. Rong-Song Jih
Teledyne Geotech
314 Montgomery Street
Alexandria, VA 22314

Prof. Lane R. Johnson
Seismographic Station
University of California
Berkeley, CA 94720

Dr. Richard LaCoss
MIT-Lincoln Laboratory
M-200B
P. O. Box 73
Lexington, MA 02173-0073 (3 copies)

Prof Fred K. Lamb
University of Illinois at Urbana-Champaign
Department of Physics
1110 West Green Street
Urbana, IL 61801

Prof. Charles A. Langston
Geosciences Department
403 Deike Building
The Pennsylvania State University
University Park, PA 16802

Prof. Thorne Lay
Institute of Tectonics
Earth Science Board
University of California, Santa Cruz
Santa Cruz, CA 95064

Prof. Arthur Lerner-Lam
Lamont-Doherty Geological Observatory
of Columbia University
Palisades, NY 10964

Dr. Christopher Lynnes
Teledyne Geotech
314 Montgomery Street
Alexandria, VA 22314

Professor Peter E. Malin
Department of Geology
Old Chemistry Building
Duke University
Durham, NC 27706

Dr. Randolph Martin, III
New England Research, Inc.
76 Olcott Drive
White River Junction, VT 05001

Prof. Thomas V. McEvilly
Seismographic Station
University of California
Berkeley, CA 94720

Dr. Keith L. McLaughlin
S-CUBED
A Division of Maxwell Laboratory
P.O. Box 1620
La Jolla, CA 92038-1620

Prof. William Menke
Lamont-Doherty Geological Observatory
of Columbia University
Palisades, NY 10964

Stephen Miller
SRI International
333 Ravenswood Avenue
Box AF 116
Menlo Park, CA 94025-3493

Prof. Bernard Minster
IGPP, A-025
Scripps Institute of Oceanography
University of California, San Diego
La Jolla, CA 92093

Prof. Brian J. Mitchell
Department of Earth & Atmospheric Sciences
St. Louis University
St Louis, MO 63156

Mr. Jack Murphy
S-CUBED, A Division of Maxwell Laboratory
11800 Sunrise Valley Drive
Suite 1212
Reston, VA 22091 (2 copies)

Prof John A. Orcutt
IGPP, A-025
Scripps Institute of Oceanography
University of California, San Diego
La Jolla, CA 92093

Prof Keith Priestley
University of Cambridge
Bullard Labs, Dept. of Earth Sciences
Madingley Rise, Madingley Rd.
Cambridge CB3 OEZ, ENGLAND

Dr. Jay J. Pulli
Radix Systems, Inc.
2 Taft Court, Suite 203
Rockville, MD 20850

Prof. Paul G. Richards
Lamont Doherty Geological Observatory
of Columbia University
Palisades, NY 10964

Dr. Wilmer Rivers
Teledyne Geotech
314 Montgomery Street
Alexandria, VA 22314

Prof Charles G. Sammis
Center for Earth Sciences
University of Southern California
University Park
Los Angeles, CA 90089-0741

Prof. Christopher H. Scholz
Lamont-Doherty Geological Observatory
of Columbia University
Palisades, NY 10964

Thomas J. Sereno, Jr.
Science Application Int'l Corp.
10260 Campus Point Drive
San Diego, CA 92121

Prof David G. Simpson
Lamont-Doherty Geological Observatory
of Columbia University
Palisades, NY 10964

Dr. Jeffrey Stevens
S-CUBED
A Division of Maxwell Laboratory
P.O. Box 1620
La Jolla, CA 92038-1620

Prof. Brian Stump
Institute for the Study of Earth & Man
Geophysical Laboratory
Southern Methodist University
Dallas, TX 75275

Prof. Jeremiah Sullivan
University of Illinois at Urbana-Champaign
Department of Physics
1110 West Green Street
Urbana, IL 61801

Prof. Clifford Thurber
University of Wisconsin-Madison
Department of Geology & Geophysics
1215 West Dayton Street
Madison, WS 53706

Prof. M. Nafi Toksoz
Earth Resources Lab
Massachusetts Institute of Technology
42 Carleton Street
Cambridge, MA 02142

Prof. John E. Vidale
University of California at Santa Cruz
Seismological Laboratory
Santa Cruz, CA 95064

Prof. Terry C. Wallace
Department of Geosciences
Building #77
University of Arizona
Tucson, AZ 85721

Dr. William Wortman
Mission Research Corporation
735 State Street
P. O. Drawer 719
Santa Barbara. CA 93102

Dr. Monem Abdel-Gawad
Rockwell International Science Center
1049 Camino Dos Rios
Thousand Oaks, CA 91360

Prof Keiiti Aki
Center for Earth Sciences
University of Southern California
University Park
Los Angeles, CA 90089-0741

Prof. Shelton S. Alexander
Geosciences Department
403 Deike Building
The Pennsylvania State University
University Park, PA 16802

Dr. Kenneth Anderson
BBNSTC
Mail Stop 14/1B
Cambridge, MA 02238

Dr. Ralph Archuleta
Department of Geological Sciences
University of California at Santa Barbara
Santa Barbara, CA 93102

Dr. Jeff Barker
Department of Geological Sciences
State University of New York
at Binghamton
Vestal, NY 13901

Dr. Susan Beck
Department of Geosciences
Bldg. # 77
University of Arizona
Tucson, AZ 85721

Dr. T.J. Bennett
S-CUBED
A Division of Maxwell Laboratory
11800 Sunrise Valley Drive, Suite 1212
Reston, VA 22091

Mr. William J. Best
907 Westwood Drive
Vienna, VA 22180

Dr N. Biswas
Geophysical Institute
University of Alaska
Fairbanks, AK 99701

Dr. G.A. Bollinger
Department of Geological Sciences
Virginia Polytechnical Institute
21044 Derring Hall
Blacksburg, VA 24061

Dr. Stephen Bratt
Center for Seismic Studies
1300 North 17th Street
Suite 1450
Arlington, VA 22209

Michael Browne
Teledyne Geotech
3401 Shiloh Road
Garland, TX 75041

Mr Roy Burger
1221 Serry Road
Schenectady, NY 12309

Dr. Robert Burridge
Schlumberger-Doll Research Center
Old Quarry Road
Ridgefield, CT 06877

Dr. W. Winston Chan
Teledyne Geotech
314 Montgomery Street
Alexandria, VA 22314-1581

Dr. Theodore Cherry
Science Horizons, Inc.
710 Encinitas Blvd., Suite 200
Encinitas, CA 92024 (2 copies)

Prof. Jon F. Claerbout
Department of Geophysics
Stanford University
Stanford, CA 94305

Prof. Robert W. Clayton
Seismological Laboratory
Division of Geological & Planetary Sciences
California Institute of Technology
Pasadena, CA 91125

Prof. F. A Dahlen
Geological and Geophysical Sciences
Princeton University
Princeton, NJ 08544-0636

Mr. Charles Doll
Earth Resources Laboratory
Massachusetts Institute of Technology
42 Carleton St.
Cambridge, MA 02142

Prof. Adam Dziewonski
Hoffman Laboratory
Harvard University
20 Oxford St
Cambridge, MA 02138

Prof John Ebel
Department of Geology & Geophysics
Boston College
Chestnut Hill, MA 02167

Eric Fielding
SNEE Hall
INSTOC
Cornell University
Ithaca, NY 14853

Dr. John Foley
GL/LWH
Hanscom AFB, MA 01731-5000

Prof. Donald Forsyth
Department of Geological Sciences
Brown University
Providence, RI 02912

Dr. Cliff Frolich
Institute of Geophysics
8701 North Mopac
Austin, TX 78759

Dr Anthony Gangi
Texas A&M University
Department of Geophysics
College Station, TX 77843

Dr Freeman Gilbert
IGPP, A-025
Scripps Institute of Oceanography
University of California
La Jolla, CA 92093

Mr. Edward Giller
Pacific Sierra Research Corp.
1401 Wilson Boulevard
Arlington, VA 22209

Dr. Jeffrey W. Given
SAIC
10260 Campus Point Drive
San Diego, CA 92121

Prof. Stephen Grand
University of Texas at Austin
Department of Geological Sciences
Austin, TX 78713-7909

Prof. Roy Greenfield
Geosciences Department
403 Deike Building
The Pennsylvania State University
University Park, PA 16802

Dan N. Hagedorn
Battelle
Pacific Northwest Laboratories
Battelle Boulevard
Richland, WA 99352

Dr. James Hannon
Lawrence Livermore National Laboratory
P. O. Box 808
Livermore, CA 94550

Prof. Robert B. Herrmann
Dept. of Earth & Atmospheric Sciences
St. Louis University
St. Louis, MO 63156

Ms. Heidi Houston
Seismological Laboratory
University of California
Santa Cruz, CA 95064

Kevin Hutchenson
Department of Earth Sciences
St. Louis University
3507 Laclede
St. Louis, MO 63103

Dr. Hans Israelsson
Center for Seismic Studies
1300 N. 17th Street, Suite 1450
Arlington, VA 22209-2308

Prof. Thomas H. Jordan
Department of Earth, Atmospheric
and Planetary Sciences
Massachusetts Institute of Technology
Cambridge, MA 02139

Prof. Alan Kafka
Department of Geology & Geophysics
Boston College
Chestnut Hill, MA 02167

Robert C. Kemerait
ENSCO, Inc.
445 Pineda Court
Melbourne, FL 32940

William Kikendall
Teledyne Geotech
3401 Shiloh Road
Garland, TX 75041

Prof. Leon Knopoff
University of California
Institute of Geophysics & Planetary Physics
Los Angeles, CA 90024

Prof. L. Timothy Long
School of Geophysical Sciences
Georgia Institute of Technology
Atlanta, GA 30332

Dr. Gary McCartor
Department of Physics
Southern Methodist University
Dallas, TX 75275

Prof. Art McGarr
Mail Stop 977
Geological Survey
345 Middlefield Rd.
Menlo Park, CA 94025

Dr George Mellman
Sierra Geophysics
11255 Kirkland Way
Kirkland, WA 98033

Prof. John Nabelek
College of Oceanography
Oregon State University
Corvallis, OR 97331

Prof. Geza Nagy
University of California, San Diego
Department of Ames, M.S. B-010
La Jolla, CA 92093

Dr. Keith K. Nakanishi
Lawrence Livermore National Laboratory
L-205
P. O. Box 808
Livermore, CA 94550

Dr Bao Nguyen
GL/LWH
Hanscom AFB, MA 01731-5000

Prof. Amos Nur
Department of Geophysics
Stanford University
Stanford, CA 94305

Prof. Jack Oliver
Department of Geology
Cornell University
Ithaca, NY 14850

Dr. Kenneth Olsen
P. O. Box 1273
Linwood, WA 98046-1273

Howard J. Patton
Lawrence Livermore National Laboratory
L-205
P. O Box 808
Livermore, CA 94550

Prof. Robert Phinney
Geological & Geophysical Sciences
Princeton University
Princeton, NJ 08544-0636

Dr. Paul Pomeroy
Rondout Associates
P.O. Box 224
Stone Ridge, NY 12484

Dr. Jay Pulli
RADIX System, Inc.
2 Taft Court, Suite 203
Rockville, MD 20850

Dr. Norton Rimer
S-CUBED
A Division of Maxwell Laboratory
P O Box 1620
La Jolla, CA 92038-1620

Prof. Larry J. Ruff
Department of Geological Sciences
1006 C.C. Little Building
University of Michigan
Ann Arbor, MI 48109-1063

Dr Richard Sailor
TASC Inc
55 Walkers Brook Drive
Reading, MA 01867

Dr Susan Schwartz
Institute of Tectonics
1156 High St.
Santa Cruz, CA 95064

John Sherwin
Teledyne Geotech
3401 Shiloh Road
Garland, TX 75041

Dr. Matthew Sibol
Virginia Tech
Seismological Observatory
4044 Derring Hall
Blacksburg, VA 24061-0420

Dr. Albert Smith
Lawrence Livermore National Laboratory
L-205
P. O. Box 808
Livermore, CA 94550

Prof Robert Smith
Department of Geophysics
University of Utah
1400 East 2nd South
Salt Lake City, UT 84112

Dr. Stewart W. Smith
Geophysics AK-50
University of Washington
Seattle, WA 98195

Donald L. Springer
Lawrence Livermore National Laboratory
L-205
P O. Box 808
Livermore, CA 94550

Dr. George Sutton
Rondout Associates
P.O. Box 224
Stone Ridge, NY 12484

Prof. L. Sykes
Lamont-Doherty Geological Observatory
of Columbia University
Palisades, NY 10964

Prof. Pradeep Talwani
Department of Geological Sciences
University of South Carolina
Columbia, SC 29208

Dr. David Taylor
ENSCO, Inc.
445 Pineda Court
Melbourne, FL 32940

Dr. Steven R. Taylor
Lawrence Livermore National Laboratory
L-205
P. O. Box 808
Livermore, CA 94550

Professor Ta-Liang Teng
Center for Earth Sciences
University of Southern California
University Park
Los Angeles, CA 90089-0741

Dr. R.B. Tittmann
Rockwell International Science Center
1049 Camino Dos Rios
P.O. Box 1085
Thousand Oaks, CA 91360

Dr. Gregory van der Vink
IRIS, Inc.
1616 North Fort Myer Drive
Suite 1440
Arlington, VA 22209

Professor Daniel Walker
University of Hawaii
Institute of Geophysics
Honolulu, HI 96822

William R. Walter
Seismological Laboratory
University of Nevada
Reno, NV 89557

Dr. Raymond Willeman
GL/LWH
Hanscom AFB, MA 01731-5000

Dr. Gregory Wojcik
Weidlinger Associates
4410 El Camino Real
Suite 110
Los Altos, CA 94022

Dr. Lorraine Wolf
GL/LWH
Hanscom AFB, MA 01731-5000

Prof. Francis T. Wu
Department of Geological Sciences
State University of New York
at Binghamton
Vestal, NY 13901

Dr. Gregory B. Young
ENSCO, Inc.
5400 Port Royal Road
Springfield, VA 22151-2388

Dr. Eileen Vergino
Lawrence Livermore National Laboratory
L-205
P. O. Box 808
Livermore, CA 94550

J. J. Zucca
Lawrence Livermore National Laboratory
P. O. Box 808
Livermore, CA 94550

Dr. Ralph Alewine III
DARPA/NMRO
1400 Wilson Boulevard
Arlington, VA 22209-2308

Mr. James C Battis
GL/LWH
Hanscom AFB, MA 01731-5000

Dr Robert Blandford
AFTAC/TT
Center for Seismic Studies
1300 North 17th St., Suite 1450
Arlington, VA 22209-2308

Eric Chael
Division 9241
Sandia Laboratory
Albuquerque, NM 87185

Dr. John J. Cipar
GL/LWH
Hanscom AFB, MA 01731-5000

Cecil Davis
Group P-15, Mail Stop D406
P.O. Box 1663
Los Alamos National Laboratory
Los Alamos, NM 87544

Mr. Jeff Duncan
Office of Congressman Markey
2133 Rayburn House Bldg.
Washington, DC 20515

Dr. Jack Evernden
USGS - Earthquake Studies
345 Middlefield Road
Menlo Park, CA 94025

Art Frankel
USGS
922 National Center
Reston, VA 22092

Dr. Dale Glover
DIA/DT-1B
Washington, DC 20301

Dr. T. Hanks
USGS
Nat'l Earthquake Research Center
345 Middlefield Road
Menlo Park, CA 94025

Paul Johnson
ESS-4, Mail Stop J979
Los Alamos National Laboratory
Los Alamos, NM 87545

Janet Johnston
GL/LWH
Hanscom AFB, MA 01731-5000

Dr. Katharine Kadinsky-Cade
GL/LWH
Hanscom AFB, MA 01731-5000

Ms. Ann Kerr
IGPP, A-025
Scripps Institute of Oceanography
University of California, San Diego
La Jolla, CA 92093

Dr. Max Koontz
US Dept of Energy/DP 5
Forrestal Building
1000 Independence Avenue
Washington, DC 20585

Dr. W.H.K. Lee
Office of Earthquakes, Volcanoes,
& Engineering
345 Middlefield Road
Menlo Park, CA 94025

Dr. William Leith
U.S. Geological Survey
Mail Stop 928
Reston, VA 22092

Dr. Richard Lewis
Director, Earthquake Engineering & Geophysics
U.S. Army Corps of Engineers
Box 631
Vicksburg, MS 39180

James F. Lewkowicz
GL/LWH
Hanscom AFB, MA 01731-5000

Mr. Alfred Lieberman
ACDA/VI-OA'State Department Bldg
Room 5726
320 - 21st Street, NW
Washington, DC 20451

Stephen Mangino
GL/LWH
Hanscom AFB, MA 01731-5000

Dr. Robert Masse
Box 25046, Mail Stop 967
Denver Federal Center
Denver, CO 80225

Art McGarr
U.S. Geological Survey, MS-977
345 Middlefield Road
Menlo Park, CA 94025

Richard Morrow
ACDA/VI, Room 5741
320 21st Street N.W
Washington, DC 20451

Dr. Carl Newton
Los Alamos National Laboratory
P.O. Box 1663
Mail Stop C335, Group ESS-3
Los Alamos, NM 87545

Dr. Kenneth H. Olsen
Los Alamos Scientific Laboratory
P. O. Box 1663
Mail Stop D-406
Los Alamos, NM 87545

Mr. Chris Paine
Office of Senator Kennedy
SR 315
United States Senate
Washington, DC 20510

Colonel Jerry J. Perrizo
AFOSR/NP, Building 410
Bolling AFB
Washington, DC 20332-6448

Dr. Frank F. Pilotte
HQ AFTAC/TT
Patrick AFB, FL 32925-6001

Katie Poley
CIA-ACIS/TMC
Room 4X16NHB
Washington, DC 20505

Mr. Jack Rachlin
U.S. Geological Survey
Geology, Rm 3 C136
Mail Stop 928 National Center
Reston, VA 22092

Dr. Robert Reinke
WL/NTESG
Kirtland AFB, NM 87117-6008

Dr. Byron Ristvet
HQ DNA, Nevada Operations Office
Attn: NVCG
P.O. Box 98539
Las Vegas, NV 89193

Dr. George Rothe
HQ AFTAC/TTR
Patrick AFB, FL 32925-6001

Dr. Alan S. Ryall, Jr.
DARPA/NMRO
1400 Wilson Boulevard
Arlington, VA 22209-2308

Dr. Michael Shore
Defense Nuclear Agency/SPSS
6801 Telegraph Road
Alexandria, VA 22310

Mr. Charles L. Taylor
GL/LWG
Hanscom AFB, MA 01731-5000

Dr. Larry Turnbull
CIA-OSWR/NED
Washington DC 20505

Dr. Thomas Weaver
Los Alamos National Laboratory
P.O. Box 1663, Mail Stop C335
Los Alamos, NM 87545

GL/SULL
Research Library
Hanscom AFB , MA 01731-5000 (2 copies)

Secretary of the Air Force
(SAFRD)
Washington, DC 20330

Office of the Secretary Defense
DDR & E
Washington, DC 20330

HQ DNA
Attn: Technical Library
Washington, DC 20305

DARPA/RMO/RETRIEVAL
1400 Wilson Boulevard
Arlington, VA 22209

DARPA/RMO/Security Office
1400 Wilson Boulevard
Arlington, VA 22209

Geophysics Laboratory
Attn: XO
Hanscom AFB, MA 01731-5000

Geophysics Laboratory
Attn: LW
Hanscom AFB, MA 01731-5000

DARPA/PM
1400 Wilson Boulevard
Arlington, VA 22209

Defense Technical Information Center
Cameron Station
Alexandria, VA 22314 (5 copies)

Defense Intelligence Agency
Directorate for Scientific & Technical Intelligence
Attn: DT1B
Washington, DC 20340-6158

AFTAC/CA
(STINFO)
Patrick AFB, FL 32925-6001

TACTEC
Battelle Memorial Institute
505 King Avenue
Columbus, OH 43201 (Final Report Only)

Dr. Ramon Cabre, S.J.
Observatorio San Calixto
Casilla 5939
La Paz, Bolivia

Prof. Hans-Peter Harjes
Institute for Geophysik
Ruhr University/Bochum
P.O. Box 102148
4630 Bochum 1, FRG

Prof. Eystein Husebye
NTNF/NORSAR
P.O. Box 51
N-2007 Kjeller, NORWAY

Prof. Brian L.N. Kennett
Research School of Earth Sciences
Institute of Advanced Studies
G.P.O. Box 4
Canberra 2601, AUSTRALIA

Dr. Bernard Massinon
Societe Radiomana
27 rue Claude Bernard
75005 Paris, FRANCE (2 Copies)

Dr. Pierre Mecheler
Societe Radiomana
27 rue Claude Bernard
75005 Paris, FRANCE

Dr. Svein Mykkeltveit
NTNF/NORSAR
P.O. Box 51
N-2007 Kjeller, NORWAY (3 copies)

Dr Peter Basham
Earth Physics Branch
Geological Survey of Canada
1 Observatory Crescent
Ottawa, Ontario, CANADA K1A 0Y3

Dr Eduard Berg
Institute of Geophysics
University of Hawaii
Honolulu, HI 96822

Dr. Michel Bouchon
I R I G.M.-B P 68
38402 St Martin D'Heres
Cedex, FRANCE

Dr Hilmar Bungum
NTNF/NORSAR
P O Box 51
N-2007 Kjeller, NORWAY

Dr Michel Campillo
Observatoire de Grenoble
I.R.I.G.M.-B P. 53
38041 Grenoble, FRANCE

Dr Kin Yip Chun
Geophysics Division
Physics Department
University of Toronto
Ontario, CANADA M5S 1A7

Dr. Alan Douglas
Ministry of Defense
Blacknest, Brimpton
Reading RG7-4RS, UNITED KINGDOM

Dr Roger Hansen
NTNF/NORSAR
P.O. Box 51
N-2007 Kjeller, NORWAY

Dr. Manfred Henger
Federal Institute for Geosciences & Nat'l Res.
Postfach 510153
D-3000 Hanover 51, FRG

Ms. Eva Johannisson
Senior Research Officer
National Defense Research Inst.
P.O Box 27322
S-102 54 Stockholm, SWEDEN

Dr. Fekadu Kebede
Geophysical Observatory, Science Faculty
Addis Ababa University
P. O. Box 1176
Addis Ababa, ETHIOPIA

Dr. Tormod Kvaerna
NTNF/NORSAR
P.O. Box 51
N-2007 Kjeller, NORWAY

Dr. Peter Marshall
Procurement Executive
Ministry of Defense
Blacknest, Brimpton
Reading FG7-4RS, UNITED KINGDOM

Prof. Ari Ben-Menahem
Department of Applied Mathematics
Weizman Institute of Science
Rehovot, ISRAEL 951729

Dr. Robert North
Geophysics Division
Geological Survey of Canada
1 Observatory Crescent
Ottawa, Ontario, CANADA K1A 0Y3

Dr. Frode Ringdal
NTNF/NORSAR
P.O. Box 51
N-2007 Kjeller, NORWAY

Dr. Jorg Schlittenhardt
Federal Institute for Geosciences & Nat'l Res.
Postfach 510153
D-3000 Hannover 51, FEDERAL REPUBLIC OF GERMANY

Universita Degli Studi Di Trieste
Facolta Di Ingegneria
Istituto Di Miniere E. Geofisica Applicata, Trieste, ITALY